Nonlinear Field Enhancement factor of Carbon Nanotubes (CNTs) in Vacuum and Partial Pressure

by

Rujun Bai

A thesis submitted to the Graduate Faculty of
Auburn University
in partial fulfillment of the
requirements for the Degree of
Master of Science

Auburn, Alabama
May 05, 2013

Keywords: Carbon nanotubes, Field emission, Fowler-Norheim Curve, Sputtering Growth time, under layer

Approved by

Hulya Kirkici, Chair, Professor of Electrical and Computer Engineering
Thomas Baginski, Professor of Electrical and Computer Engineering
Robert Dean, Associate Professor of Electrical and Computer Engineering

Abstract

Carbon nanotubes (CNTs) have attracted much attention because of their unique electrical properties and their potential applications. Large aspect ratios of CNTs together with thermal conductivity high mechanical strength and chemical inert are advantageous for applications to the field emitter. In this work carbon nanotubes are studied in order to develop cold cathode materials with efficient field emission characteristics.

Randomly aligned Multi-Walled carbon nanotubes (MWCNTs) are fabricated using chemical vapor deposition (CVD) under different growth conditions. These nanotubes are then tested for their field emission characteristics at different pressures ranging from $2x10^{-7}$ Torr to $20x10^{-3}$ Torr in Helium gas. Effects of different gases at different pressure and the catalyst thickness on the field emission properties of carbon nanotubes are studied and results are presented. Fowler-Norheim (FN) plots revealed nonlinear slopes for all the samples tested in different background pressures. It is known that the slope of the FN plots gives information about the field enhancement factor of the surface. Therefore, the nonlinearity is attributed to a nonlinear field enhancement factor. This data is used in determining a proper cold cathode material to be used as a trigger electrode for pseudospark switches.

Acknowledgments

First and foremost, I would like to express sincere gratitude to my advisor Dr. Hulya Kirkici for the instruction of my study and research, for her patience, motivation and enthusiasm. Her guidance helped me throughout the research and writing of this thesis. I could not have imagined having a better advisor and mentor for me at Auburn University.

Besides my advisor, I would like to thank the rest of my thesis committee: Dr. Thomas Baginski and Dr. Robert Dean, for their help in reviewing my thesis, insightful comments and suggestions.

My sincere thanks my fellow lab mates Dr. Haitao Zhao, Mr. Chung-nan Tsai for providing the patient training and sharing their experience on running the experiment. I also thank for my friends Mr. George Hernandez who have help me to solve countless problems during the study period in Auburn University.

Lastly, and most importantly I wish to thank my parents, Shiyu Bai and Peiyan Li for their consistent support understanding and encouragement. I would like dedicate this thesis to my parents.

Table of Contents

List of Tables

List of Figurers

CHAPTER 1

INTRODUCTION

Carbon nanotubes (CNTs), a novel form of carbon, have been introduced in microelectronics a few decades ago. Since then they have rapidly been recognized as one of the most promising electron field emitters due to their unique field emission characteristics 1995 [1]. The name for the nanotube is derived from the size as the diameter of nanometer scale and they are tubular shaped. In an ideal nanotube, hexagonal network of carbon atoms are wrapped into a seamless hollow cylinder and capped or not by fullerenes-like structures. Because of their small size, carbon nanotubes exhibit many interesting and often unexpected properties, and hence there are many possibilities for using them in nanotechnology. There has been a lot of research work on the carbon nanotubes synthesis methods as well as the investigations on their electronic, mechanical, optical, and chemical characteristics. Recently, the power of carbon nanotubes as electron field emitters was already apparent due to their low turn-on fields and high current densities [2][3][4].

Carbon nanotubes occur widely in different forms depending structures, graphitizations and appearances. CNTs are classified as single-walled, double-walled and muti-walled carbon nanotubes depending on the number of the graphene sheets rolled up (Figure 1.1).

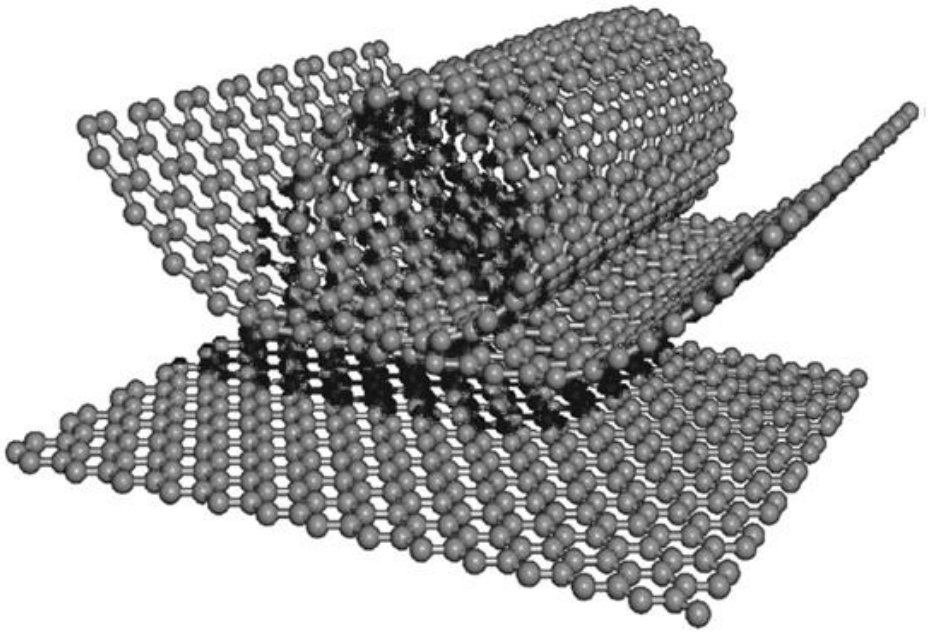

Figure 1.1: Schematic of an individual layer of honeycomb-like carbon sheet called graphene, showing the layers rolled into a CNT [5]

There have been numerous methods of synthesis carbon nanotubes. These methods for growing CNTs can be classified as carbon arc discharge method [6], laser ablation, and thermal synthesis. Within the thermal synthesis chemical vapor deposition (CVD), plasma-enhanced chemical vapor deposition (PECVD), and Flame and high-pressure carbon monoxide synthesis method can be listed [7]. All of the above methods have benefits and also disadvantages. The designed structure of CNTs determines the method of synthesis.

The unique properties of CNTs such as large aspect ratios together with high chemical stability, thermal conductivity, and high mechanical strength are advantageous for many applications. Prototype device including field emission display (FED) [8], back light units for liquid crystal display and x-ray source [3][9], electron gun for electron microscope, and microwave amplifier [10] have been

demonstrated. In the recent study, CNTs are used as cold cathode trigger electrode for a plasma switch [11]. The requirements for the CNT field emission cathodes vary significantly from device to device but we always want to have high current density with low applied voltage. In some applications we also need the field emission process under partial pressure conditions instead of high level vacuum.

My research focuses on determining the optimal synthesis conditions for better field emission performance under different test background gases (helium and dry air) by comparing the Fowler- Nordheim (FN) curve. The test background gases pressures vary from high vacuum ($5x10^{-7}$ Torr) to high pressure conditions ($20x10^{-3}$ Torr). Furthermore I compared the FN curves with respect to their growth times, sputtering times and the effects of growth conditions. My research results are on the field emission characteristics expected to support the ongoing plasma switch using CNTs as cold cathode. Result will support theory provide suggestions for fabricating CNTs with better field emission characteristics.

CHAPTER 2

CARBON NANOTUBES (CNTS)

2.1 Properties of Carbon nanotubes (CNTs)

2.1.1 Types and structural of CNTs

Carbon has several allotropes such as graphite, diamond, and amorphous carbon. Carbon nanotube was discovered by Sumio Iijima and is a form of pure carbon. A nanotube which (also known as a buckytube) is a member of the fullerene structural family. The diameter of a nanotube is on the order of a few nanometers and can be up to several micrometers in length.

Pristine SWCNTs are usually closed at both ends by fullerene-like halfspheres that contain both pentagons and hexagons. Although the growth mechanism does not suggest a carbon nanotube is actually formed like a sushi roll, the way the graphene sheet is rolled determines the fundamental properties of the tube.

Generally, the different form of CNTs can be categorized into three types by their structures, namely: Single-wall CNTs (SWCNT), Multi-wall CNTs (MWCNT), Double-wall CNTs (DWCNT). Among these three, the SWCNTs and MWCNTs are most commonly produced and used in various applications.

Single-wall CNTs: A carbon nanotube consisting of only one cylindrical graphene sheet is called single-wall nanotube (SWCNT). The Figure 2.1 shows a SWCNT with hexagonal structures which has many possibilities to form a cylinder with a single graphene sheet. The tubes are usual labeled in terms of the graphene lattice

vectors. The tube chirality can be defined in term of a chiral vector C_h which represents a possible wrapping of the two-dimensional graphene sheet into a tubular form.

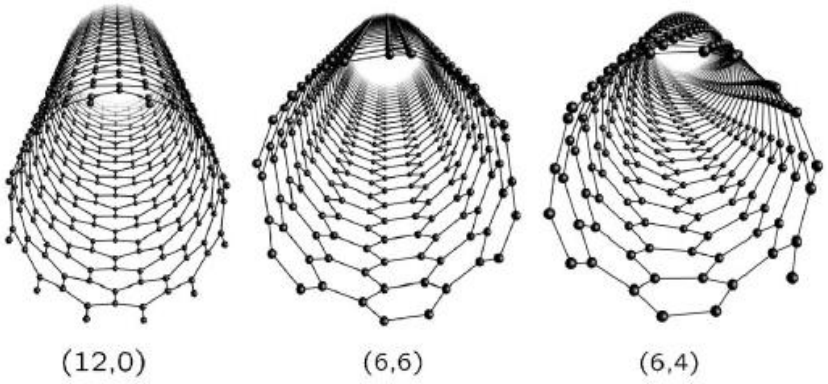

Figure 2.1: Classification of CNT based on chiral vector: (a) armchair, (b) zigzag, and (c) chiral nanotubes [12].

Multi-wall CNTs: A carbon nanotube consists of several nested cylinders with an interlayer spacing of 0.34-0.36 nm, close to the typical spacing of turbostratic graphite, called multiwall nanotube (MWCNT). In most cases, the layers of MWCNTs are chiral and of different helicities. The lengths of MWCNTs is usually well over 1um and diameters range from ~1 nm (for SWCNTs) to ~50 nm (for MWCNTs).

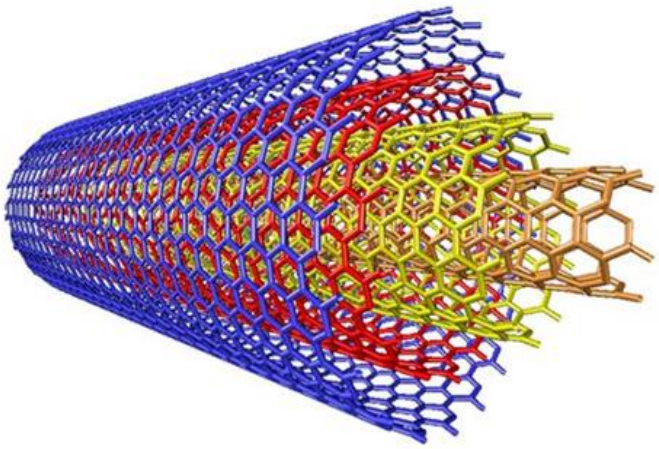

Figure 2.2: Multi walled carbon nanotubes [13].

Double-wall CNTs: A Double-wall carbon nanotubes (DWCNTs), consists of exactly two concentric cylindrical graphene layers as shown in the Figure 2.3. This double-wall structure makes DCWNTs the simplest system for studying the effects of inter-wall coupling on the physical properties of carbon nanotubes (CNTs). Compared to SCWNTs, the DWNTs have higher mechanical strength and thermal stability and also possess interesting electronic and optical properties[14]. In this thesis CNTs studied are multi-wall CNTs and synthesized by chemical vapor deposition method.

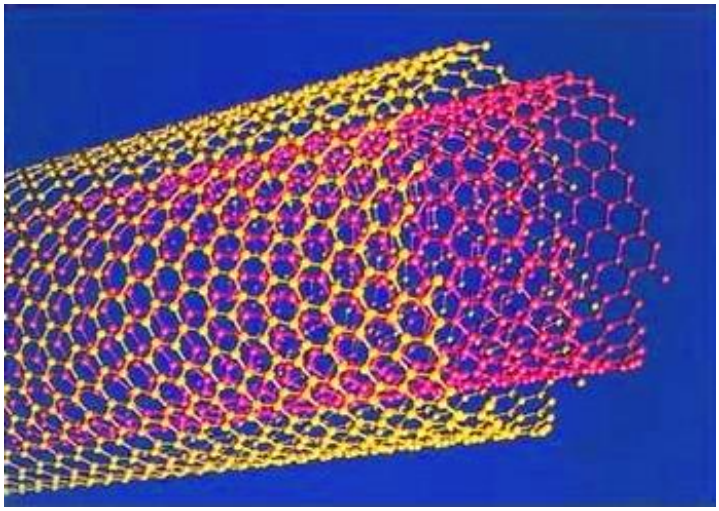

Figure 2.3: Double walled carbon nanotubes (DWCNTs) [13].

2.1.2 Electrical properties of CNTs:

The electrical properties of CNTs are sensitive with the structure of different CNTs. The band structure of graphene is quite unusual. As shown in Fig 2.4, it has states crossing the Fermi level at six points in k-spaces. The folding of the graphene layer to form a CNT introduces an additional level of quantization due to the confinement of electrons around the circumference of the nanotube [15]. So we can introduce a wave-vector k_C which is constrained by the condition

$$k_c \cdot C = 2\pi j \qquad 2.1$$

where j is integer. Thus, in going from a 2D graphene sheet to a 1D CNT, each graphene band is split into a number of 1D subbands indexed by j, with allowed energy states corresponding to slices through the graphene band structure [15].

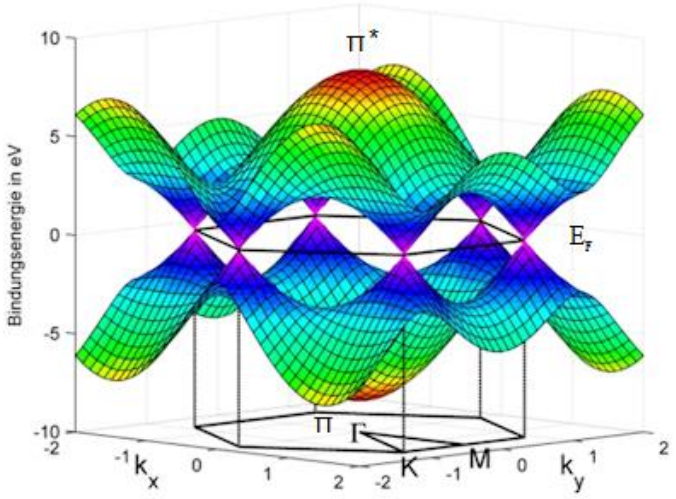

Fig 2.4: Band structure of the graphene layer [16].

Metal is known for having filled states around Fermi level. For the graphene to be metallic, the graphene K point is supposed to be among the allowed states. Otherwise the nanotube is semiconducting with a moderate band gap like the highlight point in Fig.2.5. In Fig 2.5 Lines with arrows denote reciprocal lattice vectors K_x and K_y [12].

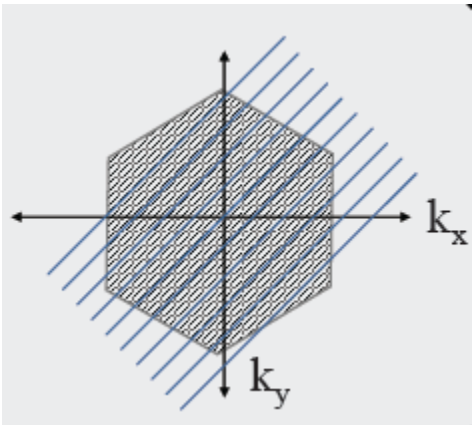

Fig 2.5: Allowed k lines onto the Brillouin zone of graphene [12].

There is a general rule for determining whether a CNT is metallic or semiconducting. Based on the chiral indices (n, m) as we described in Single-wall CNTs section are: when n=m, the tube is metallic; when n-m=3i, where i is a nonzero integer, the tube is a small-gap semiconductor; and all other combinations of (n, m) are true semiconductors [17]. The band gap of semiconducting CNTs is approximately inversely proportional to the tube diameter [18]. According to the tight-binding description of the electronic structure, as shown in Fig2.6, the band gap, E_{gap} is given by $\gamma(2a/\sqrt{3}d_{CNT})$, where γ is the hopping matrix element, the lattice constant $a=\sqrt{3}a_{cc}$ with a_{cc} being the carbon-carbon bond distance, and d_{CNT} is the nanotube diameter. a_1, a_2 are basis vectors which satisfied $a_1 = a\cdot(\frac{\sqrt{3}}{2}\hat{x}+\hat{y}), a_2 = a\cdot(\frac{\sqrt{3}}{2}\hat{x}-\hat{y})$

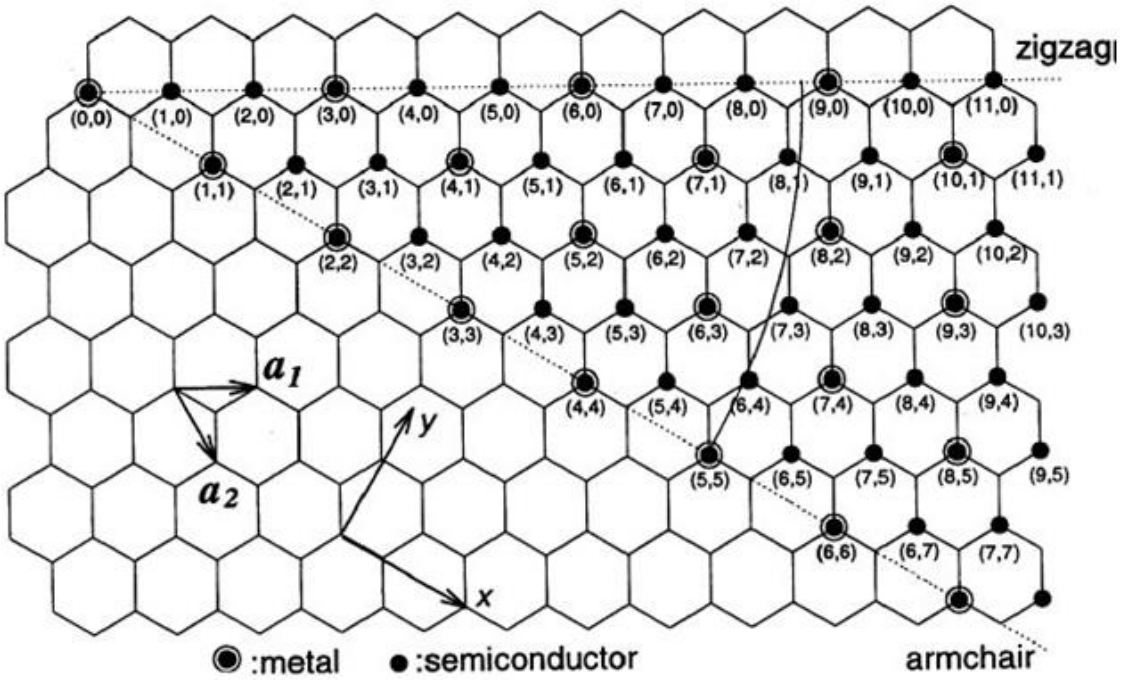

Figure 2.6: Schematic showing the folding procedure for creating nanotube cylinders from planar graphene sheets. All possible structures of SWCNTs can be formed from chiral vectors lying in the range given by this figure. (n, m) [18].

The two-terminal conductance of a metallic single-walled CNT is given by the Landauer-Buttiker formular for one-dimensional conductors:

$$G = (2e^2 / h) \cdot \sum_i^N Ti \qquad 2.2$$

where $2e^2 / h$ is the quantum unit of conductance, and T_i is the transmission of the i^{th} conducting channel. When $T_i = 1$, corresponding to the case of no scattering inside the nanotube has a resistance, $R = 1/G = h/\left(4e^2\right)$, because there are 2 contributing conductance channels near the Fermi energy.

In the case of scattering within the CNT, We use an effective scattering length, λ_{eff} to describe the scattering. Multiple processes may contribute to scattering, and thus,

$$\frac{1}{\lambda_{eff}} = \frac{1}{\lambda_{el}} + \frac{1}{\lambda_{ac}} + \frac{1}{\lambda_{op}} \qquad 2.3$$

where λ_{el} is the mean free path for elastic scattering, and λ_{ac} and λ_{op} are the mean free paths for scattering by acoustic and optical phonons, respectively [15]. Due to the one-dimensional confinement of electrons on the surface of the nanotube, which allows only forward and backward motion, and the requirements of energy and momentum conservation, the available phase space for scattering is drastically constrained. The result is weak elastic scattering, with λ_{el} >1um, in the bulk of pure metallic CNTs. Acoustic phonons contribute weakly to inelastic scattering as well, with λ_{ac} ~1um. Thus, transport in metallic phonons can scatter efficiently once carriers exceed optical phonon energies. This can result in current saturation at elevated bias and can lead to nanotube breakdown. Thus far, there is somewhat less

information on scattering in semiconducting CNTs, however, there are indications that at low energies, λ_{eff} is of order a few hundred nanometers.

For the case of a CNT device in which a semiconducting nanotube is connected to metallic leads, there are other sources of contact resistance in addition to the Landauer resistance mentioned above: Schottky barriers form at the metal/nanotube junctions, through which carriers must tunnel performance of CNT-based transistors, as will be discussed below. Additional sources of series resistance, which are not intrinsic to the device to the device itself, can in some instances make an overwhelming contribution to the total measured CNT resistance, as well [19].

2.1.3 Chemical, Mechanical, and Magnetic properties of CNTs

Besides the electronic characteristic which we have introduce in detail, it also have may many unique properties such as chemical mechanical and magnetic properties.

Chemical properties of CNTs: Chemical functionalization of CNTs is the most widely used strategy in the application of CNT-based electrochemical biosensors [20]. Chemical functionalization is not part of this thesis and will not be discussed. Carbon nanotubes exhibit low chemical reactivity. Oxidation of carbon nanotubes is one of the important chemical reactions when they undergo at high temperatures of more than 750ºC. The oxidation takes place from the tips of CNTs and inward layer by layer [21][22] which results open and thinner tubes. The open nanotubes can also be achieved by oxidizing the CNTs with strong acids in liquid phase. Huira et.al.[23] reported that different oxides groups such as carbonyl (-CO), and hydroxylic (-COH), carboxylic (-COOH) covers the surface of the nanotube after oxidation

which in turn improve the chemical reactivity of CNTs and modify their wetting properties [24].

Mechanical properties of CNTs: Carbon nanotubes are the materials with highest mechanical strength since CNTs are seamlessly rolled-up graphene layers. The mechanical properties of a material in the linear regime are commonly specified by the definition of a series of modulus (elastic constants, Young's modulus, Poisson ratio, etc.) which have been traditionally defined in a macroscopic context. The average value of Young's modulus for nanotubes is supposed to be around 1.8 TPa which is very high compare to the maximum value of the Young's modulus of steel 0.186 TPa [25].

Magnetic properties of CNTs: Another unique properties of carbon nanotubes is whether they are metallic can be controlled by an external magnetic field. A carbon nanotube can be either semiconducting or metallic, affected by the strength of the applied field, and its band gap is predicted to be an oscillatory function of magnetic field with period $\phi_0 = h/e$ [15]. Thus, metallic tubes can be made semiconducting by applying magnetic field parallel to the tube axis, and semiconducting tubes can become metallic in ultrahigh magnetic field. These magnetic effects can be explained by the modulation of the electronic wave function along the tube circumference by the Aharonov-Bohm phase [26].

2.2 Synthesis of CNTs:

Arc-discharge, laser ablation, and chemical vapor deposition have been the three main methods used for carbon nanotube synthesis. The first two employ solid-state carbon precursors to provide carbon sources needed for nanotube growth and involve carbon vaporization at high temperatures (thousands of degrees Celsius).

These methods are well established in producing high-quality and nearly perfect nanotubes, despite large amounts of byproducts associated with them and low production yield.

Chemical vapor deposition (CVD) utilizes hydrocarbon gases as sources for carbon atoms and metal catalyst particles as "seeds" for nanotube growth that take place at relatively lower temperatures (500-1000°C) [7]. The chemical vapor deposition method is very economical, low byproduct generated during the synthesis process and large area always can be achieved.

2.2.1 Chemical vapor deposition (CVD) method

Chemical vapor deposition (CVD) is the widely used method to synthesize SWCNTs and MWCNTs. In this work, thermal chemical vapor deposition (CVD) is used to fabricate CNTs onto silicon substrate. The silicon wafers are prepared by the standard micro-processing procedures adopted by the semiconductor industry. Iron (Fe) is used as the catalyst deposited onto the wafer using a DC sputtering system. Varying sputtering times of 5 and 10 min are used resulting in different catalyst thickness. After sputtering the substrate is loaded into the CVD reactor and a mixture of acetylene and argon with 20 and 75 sccm flow-rate respectively are used as the feed gases. The growth of CNTs is carried out at a temperature of 700 to 750ºC and at a pressure of 70 Torr in the CVD furnace. The CNTs are fabricated with growth times of 10, 20, 40, 80, 120 and 240 min. Figure 2.7 shows a schematic diagram of thermal CVD apparatus in the synthesis of carbon nanotubes. Detail synthesis procedure of the CNTs used in this work is described elsewhere [11][24][27].

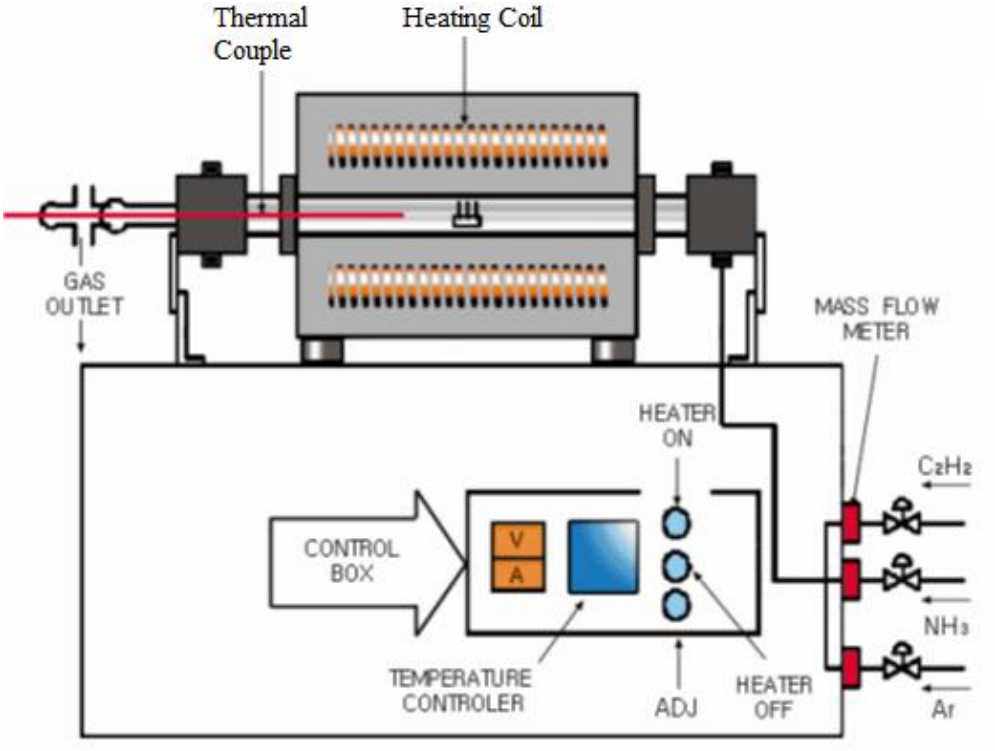

Figure 2.7: Schematic of Thermal CVD method for the synthesis of CNTs [28].

2.2.2 Growth Mechanism of CNTs

Various theories have been proposed to explain the growth mechanism of CNTs. CNT grown in CVD can be split into two basic types depending on location of the catalyst. Typically we classified them as tip-growth and base-growth. Carbon nanotube synthesis by CVD involves heating a catalyst material in a furnace and flowing a hydrocarbon gas through the tube reactor for a period of time. The catalytic species are transition-metal nanoparticles typically sputtered on high surface area materials. Simplistically, the catalyst particles serve as seeds to nucleate the growth of nanotubes. According to the Baker et.al [29] the hydrocarbon is decomposed into C_n and H on to the top surface of the metal catalyst. CNTs are supposed to be grown when these carbon fragments diffuse into the metal particle and precipitate at the other end of the particle. The catalyst particle is lifted of the surface remains on the tip of the tube during the growth process until the leading

catalytic particle is neutralized or the reaction is stopped with the hydrocarbon gas, due to the encapsulation of metal catalyst by a layer of carbon [29].

The other theory is the catalytic metal particle always remain at the bottom of the filament or tube during the growth process [29][30]. In this model the nanotubes grow from their bases unlike the first model. The bottom growth of CNTs was confirmed in many reports including Zhu and coworkers [31].

In addition, Gohiser and his co-workers investigate the relationship between the size of catalyst particles and the growth mechanic of CNTs. They examined cobalt, nickel, and iron catalyst particles. The result shows that the growth mode switches from "tip-growth" for large particles (>>5 nm) to "base-growth" for smaller ones (<5 nm). While single-walled nanotubes and those with few walls (typically <7 walls) grow from their base, larger multi-walled nanotubes are fed with carbon via their tips which support the catalyst particle [32].

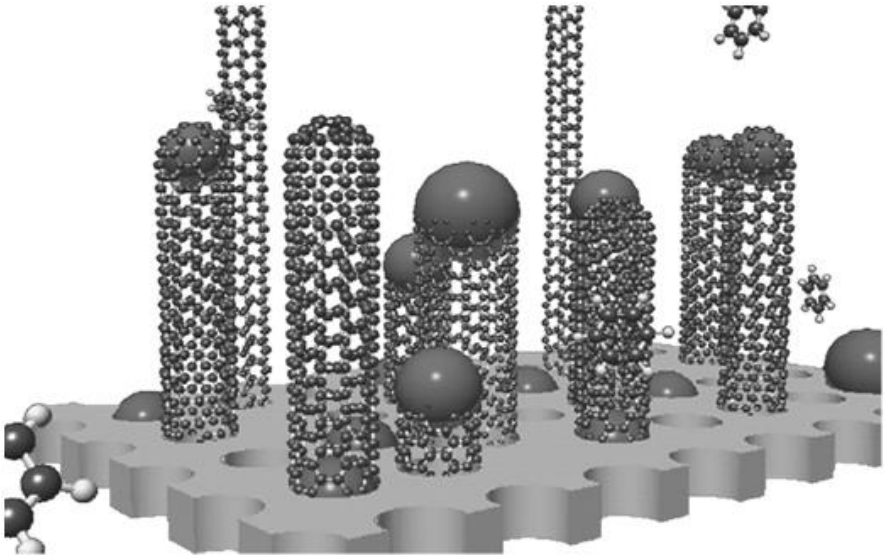

Figure 2.8: A graphical description of the tip-growth and root-growth nanotube models, in which the catalytic particles are located at the tip and at the root, respectively. Carbon species are illustrated as benzene molecules, and the base is the simplified model of the zeolite (Hayashi et al . 2003) [5]

2.3 Applications of the field emission of CNTs:

Carbon nanotubes (CNTs) exhibit excellent field emission properties due to their high aspect ratio, nanometer-sized tip radii, large effective surface area, tubular structure, light weight, strong mechanical stiffness and high thermal and electrical conductivity which will likely be prime candidates as electron sources in vacuum electronic applications. There are many applications based on the electron field emission of CNTs have been demonstrated such as vacuum microwave amplifiers, e-beam lithography, x-ray tubes and flat panel displays which require stable, uniform, and high current densities at low applied fields [33][34].

2.3.1 Electronic device applications:

CNTs for the flat panel displays were proposed as the alternative for the many other field emission displays in 1995 [24]. A fully sealed 4.5 inch emission display was produced by Samsung which the carbon nanotube-based 128 lines matrix-addressable diode display at a color mode with red, green, and blue color phosphor. The structure of panel structure of carbon nanotube-based diode-type flat panel display consists of two sets of glass plates: SWCNTs stripes on the patterned cathode glass and phosphor-coated indium-tin-oxide (ITO) stripes on the anode glass. The spacing between two sets of glass plates is kept by 200 μm space, and the pixels are formed at the intersection of cathode and anode stripes. Emission currents were characterized by the direct current (dc) mode and pulse-modulating mode at voltages up to 800 V. The pressure between the anode and cathode was evacuated down to 1×10^{-7} Torr [35] .

J.Zhang and colleagues have developed the multiplexing ratiography using a carbon nanotube based x-ray source. Their multi-pixel x-ray source, using the carbon nanotubes (CNTs) as the field emission cathode, can generate a plurality of

spatially distributed X-ray beams (pixels) with programmable intensity, pulse width, and repetition rate. The x-ray source comprised a linear array of nine CNT electron field emission cathodes, a shared common gate, electrostatic focusing optics, and a molybdenum target housed in 10^{-8} Torr vacuum. During operation the anode voltage was fixed at 40kV and the gate current was adjusted to obtain up to 1 mA tube current per pixel [33].

2.3.2 Cold cathode applications:

Most recently CNTs as a cold cathode material develop the pseudospark switch in our group. In many pulsed power and high power applications the switches need to be capable of handling high power levels about 10^{12} W range with low jitter time in the orders of 10^{-9} s. The usual conventional switches such as voltage switch gears are no longer adequate to meet these requirements [24].

The pseudospark switch also known as cold-cathode thyratron, is one of the plasma device to control high voltage (several kV to mV) and high current pulse discharges. It is a gas filled tube which operates at low pressures and capable of high speed switching. It is characterized by a very rapid breakdown phase with high hold-off voltages of several tens of kV and peak currents 10kA with pulse repetition up to several kHz. The discharge can be operated at 100% current reversal without turning into a constricted arc [24] .

Carbon nanotubes are among the best choice used for the triggering mechanism in many high power switches due to its field emission characteristics with low turn-on voltage and high current density. Beside as cold cathode material in many high voltage applications CNTs is used in pseudospark switches for the triggering mechanism.

Generally the CNTs show excellent field emission characteristics in the high vacuum conditions. The turn-on electric fields are very low with high current densities in high vacuum. However these parameters seem to be deteriorated with increase in the operating pressure levels. Different gases which were filled in the field emission tested chamber also affect the turn-on electric field and maximum current densities of nanotubes. In order to find out the optimal CNTs as a cold cathode material for pseudospark switches, we analyze the field emission performance in dry air and helium condition separately.

CHAPTER 3

FIELD EMISSION FROM SOLIDS IN VACUUM

3.1 The concepts of field emission:

Electrons can be extracted from a solid surface to vacuum mainly in two ways: one is by increasing the temperature of the solid material and the other by applying a strong electrical field. Commonly we defined the electron emission from solids by increasing the temperature of the material as thermionic emission. When the electron emission is due to the applied field without the heat, it is called the cold cathode field emission. In this case, the electrons with energies below the Fermi level predominate the emission process because the field dependence of the potential barrier shape between the material and vacuum is modified under the influence of the applied electric field [36].

This process is commonly explained by the quantum mechanical tunneling of electrons from the solid material surface to vacuum. Without the applied field, the potential barrier between the material's Fermi level, defined as the topmost filled energy level of the electron system, and the vacuum potential prevents electrons being extracted from the surface. While the material under the strong electrical field, the vacuum potential is modified, and it declines in magnitude away from the material surface and, the electronic band structure can be sketched as shown in Fig.3.1. When the applied field is strong enough, the electrons can overcome this deformed and reduced potential

barrier sufficiently and the probability of electrons tunneling though the barrier becomes significant. As a result, field emission current develops.

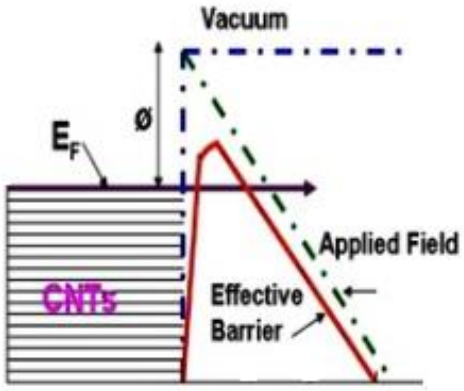

Fig. 3.1 Schematic of CNTs barrier under high electrical field (E_F is the Femi energy level, the applied electrical field is E, ϕ is the work function of the CNTs) [37]

3.2 Fowler-Nordheim theory:

3.2.1 Fowler-Nordheim tunneling :

In most applications, the field emission characteristics of materials are described by the dependency of the current flow as a function of the applied field. This is called the emission current. A reciprocal function, described below is called the Fowler-Nordheim (F-N) equation, named after the first authors to treat this effect as wave-mechanical tunneling through a triangular potential barrier. Since then Fowler-Nordheim plots become the common model to describe the field emission characteristics of solid metal in vacuum. Recent years have seen renewed interest in field electron emission, in FN theory and in the corresponding theory of field emission from semiconductor-type materials. This has largely been driven by technological interest in vacuum microelectronics and field emission displays, and by associated questions about how electrons are emitted from various materials, especially diamond-like carbon and related materials [38].

The original FN-type equation was derived from a rigorous solution for the tunneling current from cold metal surface by intense electric fields in 1928 by Fowler and Nordheim [39], based on several hypotheses and some simplifying assumptions. In their theory, Fowler and Nordheim assumed (1) a smooth, flat, planar emitter surface, with constant electric field outside it; (2) disregarded the details of emitter atomic structure; (3) ignored what would now be called the exchange-and-correlation interaction between the escaping electron and the emitter surface, and assumed tunneling took place through an exact triangular(EF) barrier; (4) a Sommerfeld-type free-electron model for the emitter electron states (and improved it by including electron spin); (5) electrons obeyed Fermi Dirac statistics; (6) approximated emitter temperature as 0 K; and (7) made various mathematical approximations. Their resulting equation gives the local emission current density J in terms of the local thermodynamic work-function ϕ of the material and the local surface electric field E_L resulted by applied field.

In summary, the Fowler and Nordheim (FN) equation is described as [40][41]:

$$J = \frac{e^2 E_L^{\,2}}{8\pi h\phi} \exp\left(-\frac{8\pi\sqrt{2me\phi^3}}{3hE_L}\right) \qquad 3.2$$

where J is the emission current density, ϕ is the work function, e is electron charge and h is Planck constant. Also, E_L is the related local field defined by $E_L = \beta E$ where E is applied electric field between the anode and the cathode satisfying $E = V/d$. (V is a potential difference which applied across two planar parallel electrodes with separation distance d) and β is the field enhancement factor.

In the literature, the parameters $a = \frac{e^2}{8\pi h} = 1.54\times10^{-6}\, AeVV^{-2}$ and $b = \frac{-8\pi\sqrt{2me}}{3h} = 6.83\times10^{9}\, eV^{-3/2}Vm^{-1}$. Using this current density equation, a

reciprocal equation, namely the FN equation is commonly used. As seen in equation (3.3) [42].

3.2.2 Fowler-Nordheim curve:

The FN equation is usually re-written as:

$$\ln(\frac{J}{E^2}) = \ln(a\Phi^{-1}\beta^2) - b\frac{\Phi^{3/2}}{\beta E} \qquad 3.3$$

This equation yields a straight line in the coordinate of $\ln(J/E^2)$ versus $1/E$ and called the FN plot of the material in question. The slope of the plot is inversely proportional to the field enhancement factor β and theoretically given by

$$k = -\frac{b\phi^{3/2}}{\beta} \qquad 3.4$$

We can easily determine the slope k from the FN plots since we use the least squares method to fit experiment data. Furthermore, if the mean work function of the material. From this, we will easily calculate the field enhancement factor β using equation 3.4. The intercept of the straight line of the FN curve is:

$$y = \ln(a\Phi^{-1}\beta^2) \qquad 3.5$$

In most cases it is considered to be a constant value during the field emission process, and is only related to the effective emission area [42].

3.3 The properties of field emission:

As previous introduced, in order to realize field emission we have to apply a strong electrical field to the material. In this research, our goal is to generate high electron density with minimum applied field. Therefore, we measure the emitted

current to determine the three parameters to evaluate the field emission performance of a material, namely: the turn-on field (E_{to}), threshold field (E_{th}) and field enhancement factors (β).

Though there is no perfect definition of the turn-on electric field and threshold electric field, they are generally defined as voltage at which the measured current density reaches to 1μA/cm² and 1mA/cm², respectively. Field enhancement factor (β) is determined based on the Fowler-Nordheim model describe above with considering the geometric effects of the field emission surface. One of the definitions of β is

$$\beta = \frac{E_L}{E} \qquad 3.6$$

E_L is the local normal surface electric field and E is the applied field[43]. The geometric of the field emission surface greatly change the local electric field. This adds difficulty in determining the field enhancement factor precisely.

In this thesis, the field emission current densities of variety of in-house grown carbon nanotubes (CNTs) are measured in vacuum. From this data, the FN curves are plotted, and field emission characteristics are determined. The field enhancement factors and turn on field of each sample is tabulated and conclusions are made. Furthermore, in this work, the lifetime of the material that is being used as field emitter is important. As the electrons extracted from the surface, the surface geometry may change with each use of the material in application. Study of the change in electron emission from the cathode surface with respect to the applied electric field over time which will influences the turn-on electric field is valuable because, as a cold cathode the turn on field and the lifetime must be considered between each use. This thesis is to study the field emission characteristics of CNTs

and commonly, we record the lifetime of CNTs in this way. First we apply some value voltage to the anode and progressively increase the voltage to until field emission curve is recorded. Once the field emission data is recorded we set the applied voltage at a constant value and measure the current during few minutes until the cathode ceases to emit [24]. These data and interpretation of the data are presented in the following sections.

3.4 The material to realize the field emission:

Generally, metals having conductive properties are assumed to be good field emission materials and conductive materials generally are chosen to realize field emission characteristic. There are some researches in studying traditionally non-conductive materials' field emission characteristics by changing the structure of the material. For example Y.W.Zhu et al have done some research on the field emission from ZnO nanoneedle arrays [44]. Shaomao Li has measured field emission characteristics of several nano-materials including CNTs, ZnO and textured Cu [45].

Due to the unique properties of carbon nanotubes (CNTs), they have been considered to be the ideal material to realize field emission. As expected, high aspect ratio lead to a high field enhancement factor β, and conductive properties reduce the barrier between the field emission surface and vacuum.

3.5 Field emission from Carbon nanotubes (CNTs)

CNTs are considered as fairly good electron emitters with high aspect ratio, among other conductive emitters. As a consequence, different geometries such as different shape of anodes and interelectrode distances and different synthesis method

like arc-discharge and CVD lead to different types such as single wall carbon nanotubes and multiple wall carbon nanotubes with different aspect ratio of CNTs. An overview of the field emission data for nearly all types of nanotubes in the literature is listed in Table 3.1. The field emission characteristics of CNTs so far are good with local electric field 1.5V/µm for SWNT and turn-on electric field around 0.75V/µm for CVD MWNT. The film surfaces used for emission are quite small (below 10^{-4} cm²). In Table 3.1 [46], d is the inter electrode distance, S the emission area, E_{to} and E_{thr} are the turn-on and threshold voltages corresponding to when the current density of 10µA/cm² and 10mA/cm² are reached. The current density $J_{\max}$ is the maximal current obtained without destruction of the emitter: (n.a.) means that the value is not indicated or could not be deduced from the figures: and (*) indicates that the value was estimated or extrapolated from the presented data.

Table 3.1: Emission characteristics of carbon nanotube films[46].

Emitter	d (µm)	S (cm^{-2})	E_{to} (V/µm)	E_{thr} (V/µm)	J_{max} (A cm^{-2})	Remarks
MWNT	10–40	0.002	n.a.	<25*	1	Very dense "tubulene" film
MWNT	15	0.003	n.a.	~15*	10	Very dense "tubulene" film
Arc MWNT	20	0.008	n.a.	20*	0.1	
Arc MWNT	30	0.007	4.0	6.5		
Arc MWNT	125	0.07	2.6	4.6		
Arc MWNT	125	0.07	1.1	2.2		Purified sample with closed caps
Arc MWNT	20–100	2.5×10^{-5}	7.5*	10*	0.4	Open tubes dispersed in epoxy
Arc MWNT	80	0.025	0.9*	4*		O_2 plasma treated tubes dispersed in epoxy
Arc MWNT	200	0.02	n.a.	1.5		Tubes dispersed in epoxy
SWNT	125	0.07	1.5	3.9		
SWNT	10–300	0.002	n.a.	4–7	4	
SWNT	150	3.1	2.1*	n.a.		
CVD MWNT	n.a.	0.001	1.7*	n.a.		
CVD MWNT	70	n.a.	n.a.	4.8–6.1		Aligned MWNTs, 15 emitters
CVD MWNT	150	3.1	n.a.	2.1*		Large amount of graphitic fragments
CVD MWNT	n.a.	0.0003	4.8	6.5	0.1–1	
CVD MWNT	600	0.07	n.a.	$\geqslant 5$		
CVD MWNT	150	0.2	3	6.6*		Si substrate
CVD MWNT	500	0.1	1.6	5*		Steel substrate
CVD MWNT	500	0.1	3	5.6*		Ni substrate
CVD MWNT	10–300	0.002	0.75	1.6	1–3	Catalyst supplied in gas phase
Graphitic fibers	300	1–10	2.1	n.a.	0.2	

The field emission current of just a single nanotube is observed to be constrained because of its very small tip diameter. Researchers have considered using array of aligned nanotubes or patterned nanotubes to improve the field emission performance. The interesting point which observed here is the high density of nanotubes at the emitting surface does not lead to high emission current density during the field emission process. This is understood because when the tube density is too high and aligned: screening of the electric field occurs [47]. Vertically aligned nanotubes pillars are considered as the ideal emitting structures with spacing among each pillar roughly equal to their height. A CNT pillar is described as a uniform, highly dense, vertically aligned, compact bundle of CNTs. Vertical self-alignment of CNTs results from the van der Waals interaction between neighboring CNTs and contribute to the excellent structural stability of CNT [7]. The CNTs at the edge of each pillar experience an enhanced electric field due to reduced field screening [48]. Beside the field screening effect, the edge effect can also change the efficiency of field emission. Shunjiro Fujii and colleagues conducted series of field emission experiments on CNT pillars [49]. They found that it would greatly enhance the field emission performance of CNTs with increasing the edge area of the CNT pillars [49]. Some research groups focus on increasing the edge area of the CNT pillars by change the format of the CNT pillars such as the ring shape pillars, square and circle shape pillars and double layers of the CNT pillars to get relatively lower turn on field and relatively higher current density [49][2][50].

Many research groups have conducted series of field emission experiments on individual nanotubes as well as SWCNT and MWCNT films having SWCNT and MWCNTs. Assuming $\Phi=4.5eV$ typical field enhancement factors calculated form F-N slope ranged from 30,000 to 50,000 for single MWCNT and from 1,000 to 3,000

for MWCNT films [51][52]. The values for E_{to} and E_{thr} were found to be as low as 0.9V/μm and 2.9V/μm respectively for these samples [49][50].

3.5.1 Fowler-Nordheim curve of ideal CNTs field emission:

According to the Fowler-Nordheim equation, from the field emission curve we obtain a straight line in the coordinate of $\ln(J/E^2)$ versus 1/E. Fig 3.1 is a representative curve of a sample studied in this thesis. The experimental data is collected in vacuum (1×10^{-7} Torr) and the MWCNTs are synthesized in-hose with 5 min sputtering time and 20 min growth time. In this study, however we found that the FN curve of CNTs field emission is not an exactly straight line as we expected. Several research groups have focused on the non-linear characteristics of the FN plot of CNTs in the literature [42][53]. This nonlinear phenomenon may be a result of different fabrication process of CNTs. One theory model is that different fabrication process will lead different types of CNTs and with each type having different field enhancement characteristics. Also, for each fabrication method will result in CNTs attaching to the substrate differently. While others believe the different contact resistant in the substrate play a significant role to the nonlinear slope [53]. So the bond between the substrate and each individual CNT strand is different having different contact to the substrate. Then the electron will tunnel through more than one barrier to overcome before emitted into vacuum [54][55]. Many researchers consider the space charge effect to explain the non-linear behavior. As the field emission current may start to saturate at some point leading a knee on the FN plot. While others assume the presence of adsorbates (adsorbed molecules or impurities) at the CNT apex that can enhance the field emission at low applied electric field, which

would be then removed at high applied electric fields, causing the current to saturate [54].

The field emission data of CNTs in the literature are mostly measured in vacuum. For real applications, high level vacuum ambiance is not possible. Most devices work in partial pressure environment. The different kinds of background gas and various pressures will great affect the emission current. So analyzing the nonlinear FN curve to find out the best fabrication condition of CNTs for field emission will be important for realistic applications.

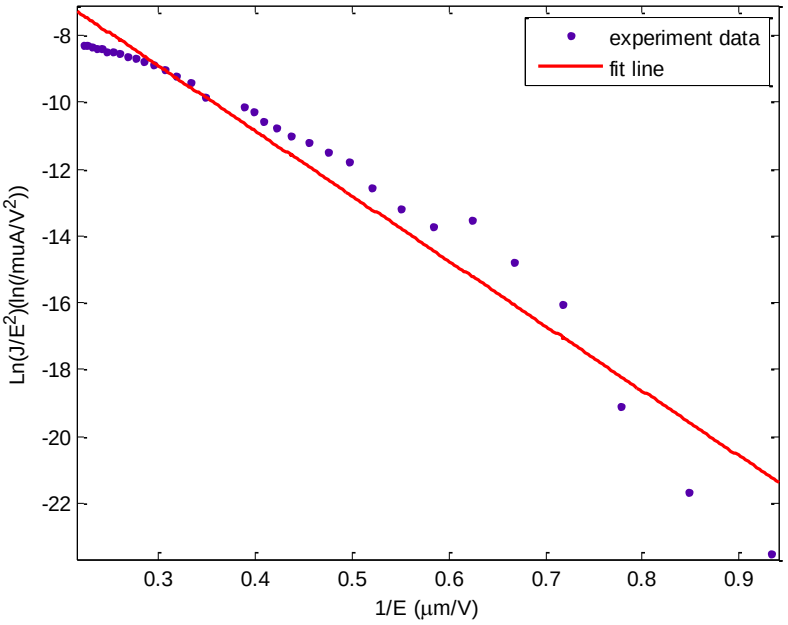

Fig 3.2 Field emission in FN coordinates of WMNTs.

3.5.2 The properties of CNTs affecting field emission:

Comparing the thermionic emission mechanism, the field emission current is mostly controlled by the external field. Also the properties of field emission material will affect the result. Through the Fowler-Nordheim (FN) equation, we see that the work function and the field enhancement factor affect the field emission

current. The work function is a basic material property that cannot vary significantly for a material. For CNTs the work function is different due to their different structures and varies from 4.5eV to 5eV for SWCNTs and MWCNTs respectively [56][57]. Additionally, all the field emission sources rely on field enhancement due to sharp tips/protrusions (aspect ratio). In a first report of electron emission from CNTs, Rinzler et al. studied field emission from an individual multi-walled nanotube (MWCNT) attached to a graphite fiber along the field direction [58]. With a bias voltage of less than 80 volts, emission currents of 0.1 to 1μA were obtained at room temperature [59].

3.5.3 The lifetime of CNTs during the field emission:

Stability of the emission currents and the degradation tests for CNTs are significant parameters to evaluate the performance of CNTs as field emission cathodes. In a previous work, gradual degradation of the emission current was always observed with time [60]. The test time usually varies from several tens of hours to several hundreds of hours. Logan T. Williams and his colleges run their gradual degradation test over than 300 hundreds hours [61]. The maximum life span of their arrayed carbon nanotube field emission cathode is 368 h and they attributed the failure mechanisms to resistive heating divided into two different modes, namely: the oxidative ablation at the root of nanotube and the field evaporation at the tip. For nanotubes where the contact resistance between the nanotube and the substrate is much higher than the resistance of the nanotube, the majority of the ohmic heating is deposited at the root. The high temperatures enhance the rate of oxidative ablation and lead to the nanotubes rupturing near the root, leading to failure. The field evaporation at the tip occurs when the resistance of the nanotube is higher than the

contact resistance between the CNTs and substrate. Then the peak temperature at the tip of the nanotube will result in the removal of one or more atoms from the nanotube rather than electrons [61]. Experiments show that the operating pressure in the testing chamber plays major role in the degradation of CNTs. This is because the excess residual gas molecules in the chamber are ionized during the aging process resulting in the destruction of the tips of nanotubes. Therefore higher vacuum conditions yield better results and more stable emission current compared to the results in poor vacuum conditions [24].

In our experiment, all the samples were tested for their lifetime and current stability by applying constant voltage of 600V at high vacuum conditions. Current densities of all the samples were plotted with respect to time to see if there is any degradation in their characteristics. In all the cases it can be observed that there was very little degradation in their emission current [24].

CHAPTER 4

RESULTS

In this thesis the analysis of field emission characteristic of randomly-oriented multi-walled carbon nanotubes grow on silicon substrates with and without under-layer is presented. The carbon nanotubes are in-house synthesized using chemical vapor deposition method. The under-layers are silicon dioxide and titanium and iron is used as the catalyst to grow the CNTs. Field emission current densities of each sample are recorded and from this data, the F-N plots are produced. By use of the two field enhancement factors model based on Fowler-Nordheim equation are determined for each sample. The synthesis process of the carbon-nanotubes is explained in [27][24] and is summarized here briefly. Silicon is used as substrate and iron is used as the catalyst for all the samples studies here. Both the iron catalyst and the titanium under-layer are deposited as thin film onto the substrate using DC sputtering system. The thickness of each layer are discussed in [27]. The silicon-oxide under-layer was already on the silicon substrate when purchased. Once the under-layer and the catalysis are formed, on the substrate, it is put in the CVD chamber. The length of the CNTs is controlled by the grow time in the CVD chamber. The length of the CNTs is controlled by the growth time in the CVD chamber. The details of growth process is also explained in [27]. The initial batch samples are with no under-layer and nanotubes are grown with different growth times namely 10 min, 20 min, 40 min, 80 min, 120 min, and 240 min, each with set of

5 min and 10 min sputtering time. These samples are tested for their field emission characteristics, first in vacuum and then under different pressure conditions in helium and dry air. Effects of gas pressures on the field emission properties are analyzed by our model. A series of field emission experiments were performed on each of these samples under different pressures to find the change in turn-on electric field and the voltage at the 'knee' location of the FN curves in our model. These results are expected to give us a theoretical support to help us to determine the optimum growth condition for high pressure field emission test environment.

Another set of samples grown on silicon substrates with silicon dioxide and titanium underlying layer are also tested for their field emission character only in vacuum condition. Comparing the field emission character of CNTs on silicon dioxide and CNTs grown without any under-layer on silicon, we can determine which substrate would be more suitable for realizing high quality field emitting material.

4.1 SEM Images of Random-Oriented CNTs

Following are the SEM images of all the samples with 5 min sputtering and 10 min sputtering. The samples with different growth time for both cases are presented with resolutions of 9000X and 30000X. The following images shows that the samples with both 5 min and 10 min sputtering consist of cluster free CNTs. The 10 min sputtering of silicon substrate with Fe after 5 minutes baking and CVD growth of CNTs has produced very good quality randomly aligned Multi Walled Carbon nanotubes (MWCNTs). The length and density of nanotubes is increased with increasing the growth period in all cases of sputtering. The notation 5-10 means sample with 5 min sputtering and 10 min growth period.

Images of CNTs with 1 min and 5 min sputtering and growth period is 20 min on silicon dioxide underlying layer with resolution of 9000X are also exhibited here. Random-Oriented MWCNTs were successfully fabricated on silicon wafer with silicon dioxide and titanium underlying layer which help us to find out the optimized fabrication condition for field emission of CNTs.

4.1.1 SEM Images of CNTs on pure silicon

4.1.1.1 Images of CNTs with 5 min sputtering:

(a) 5-10

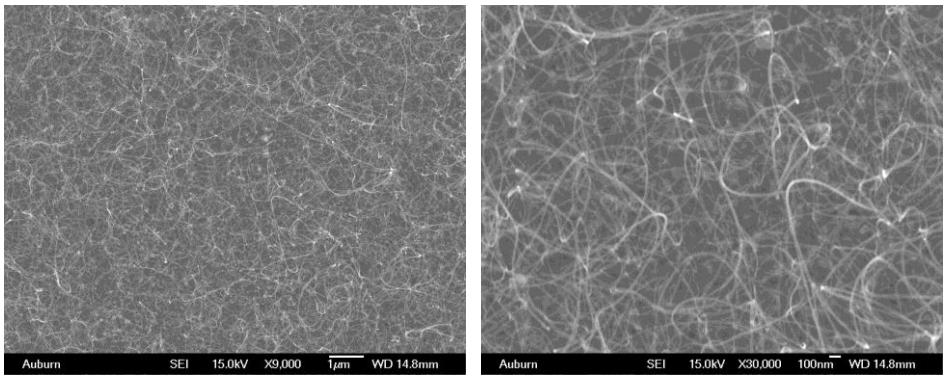

(b) 5-20

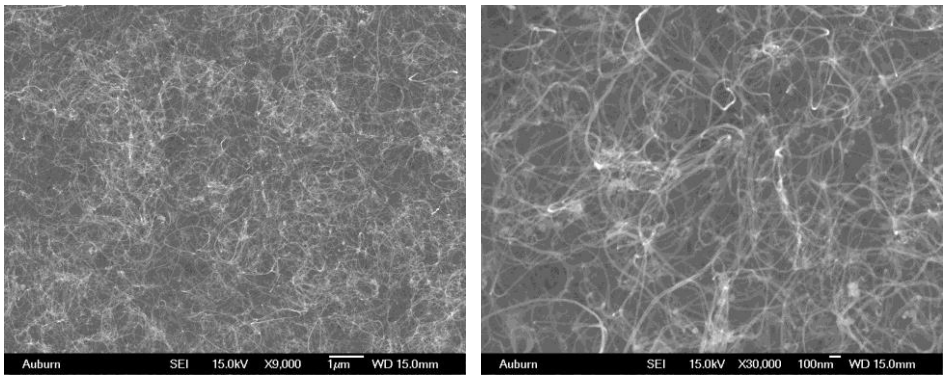

(c) 5-40

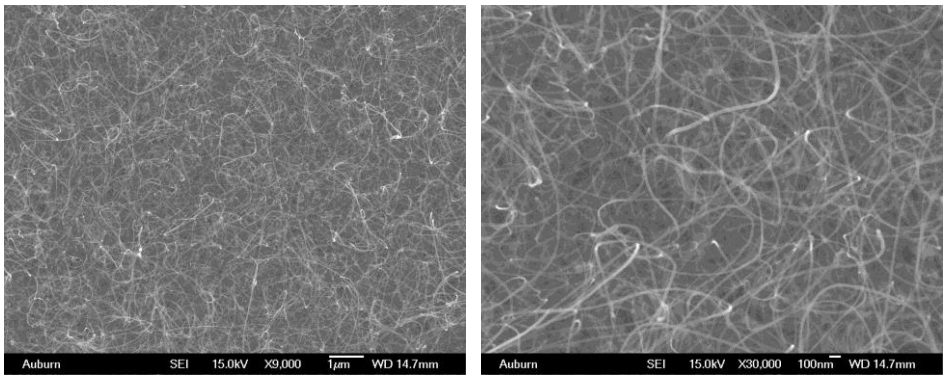

(d) 5-80

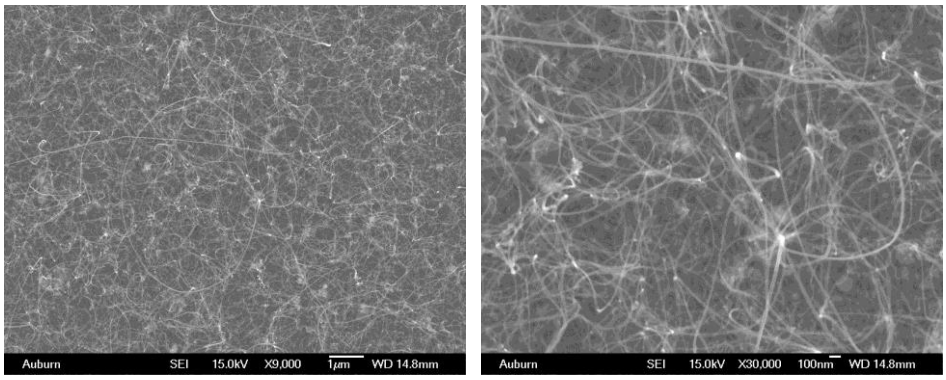

(e) 5-120

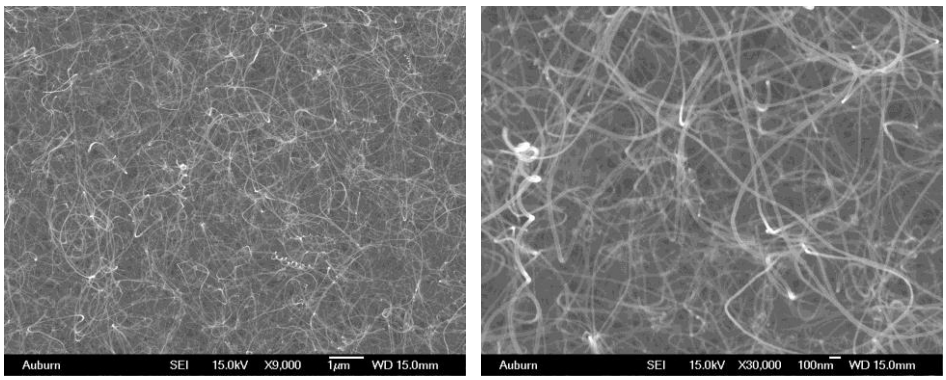

(f) 5-240

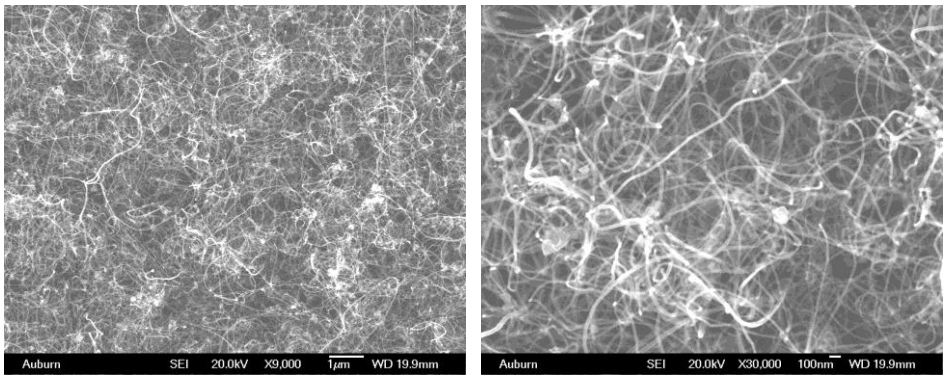

Figure 4.1: Images of CNTs with 5 min sputtering and growth periods (a) 10 min (b) 20 min (c) 40 min (d) 80 min (e) 120 min (f) 240 min each set is with resolution of 9000X and 30000X.

4.1.1.2 Images of CNTs with 10 min sputtering:

(a) 10-10

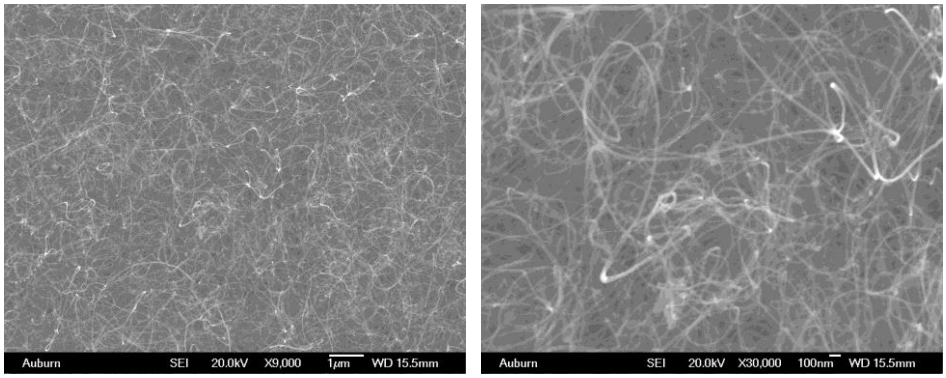

(b) 10-20

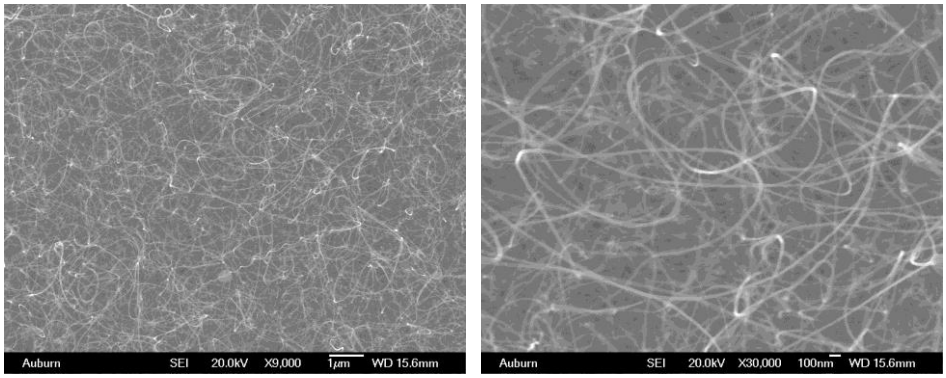

(c) 10-40

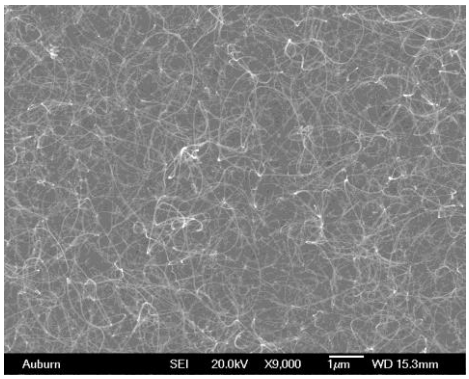

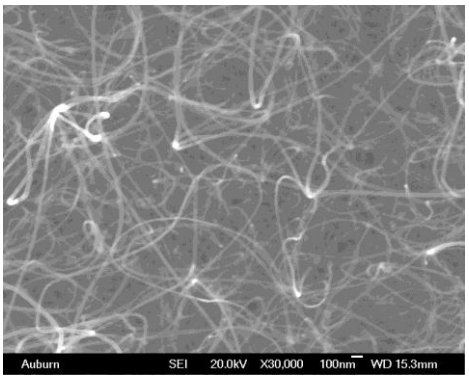

(d) 10-80

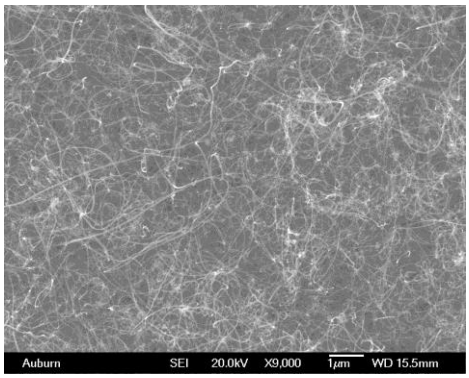

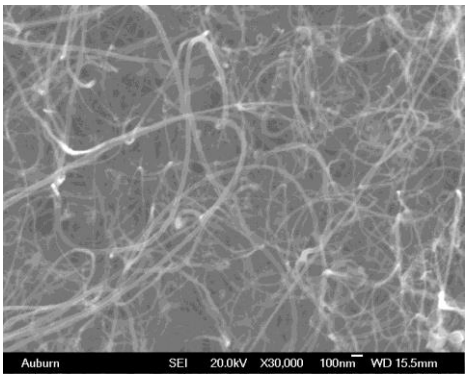

(e) 10-120

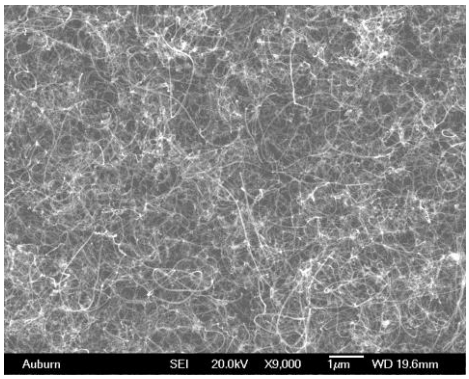

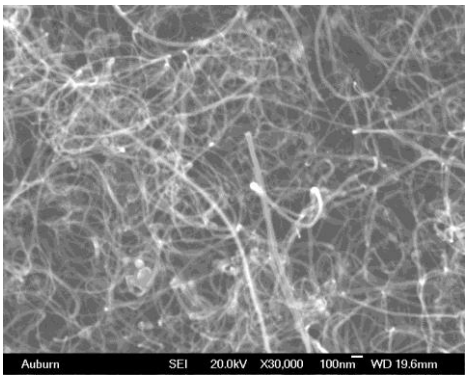

(f) 10-240

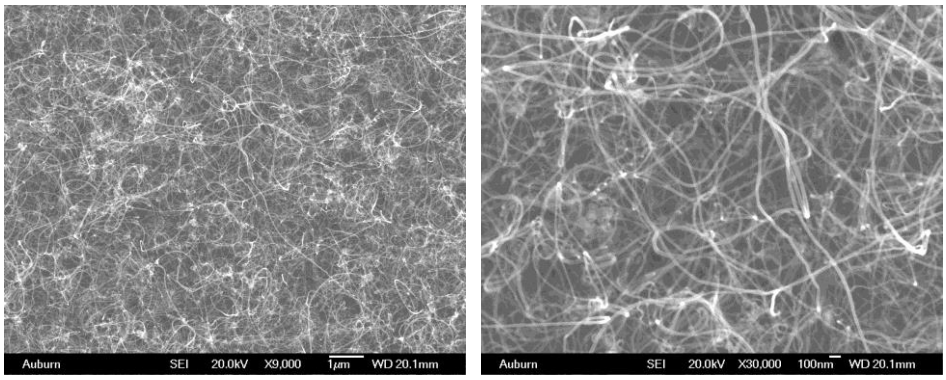

Figure 4.2: Images of CNTs with 10 min sputtering and growth periods (a) 10 min (b) 20 min (c) 40 min (d) 80 min (e) 120 min (f) 240 min. Each set is with resolution of 9000X and 30000X.

4.1.2 SEM Images of CNTs on silicon dioxide

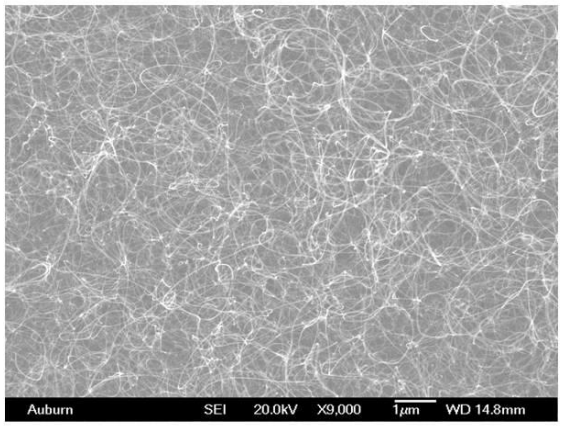

Figure 4.3: Images of CNTs with 1min sputtering and growth period is 20 min with resolution of 9000X

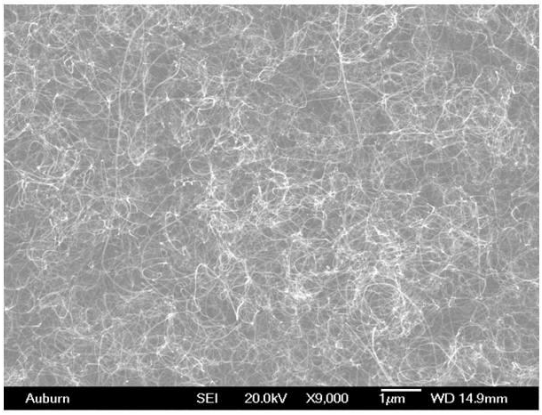

Figure 4.4: Images of CNTs with 5 min sputtering and growth period is 20 min with resolution of 9000X

4.2 Field emission measurement process

The CNT samples are loaded into the high vacuum chamber to test their field emission characteristics. The chamber is first pumped by the mechanical pump up to mTorr range and then turbo pump is used to pump down, until the pressure reaches $2x10^{-7}$- $5x10^{-7}$ Torr range. A parallel- plate set-up is used to analyze the electron field emission characteristics of carbon nanotube samples. In this experiment setup, the carbon nanotubes sample serves as the electron emitting material, placed on the cathode and a small cylindrical rod with area of collector $0.031415cm^2$ serving as the anode. The two electrodes were separated by two thin glass, the insulating spacers (the thickness of the thin glass) of width 140~150μm.

(a)

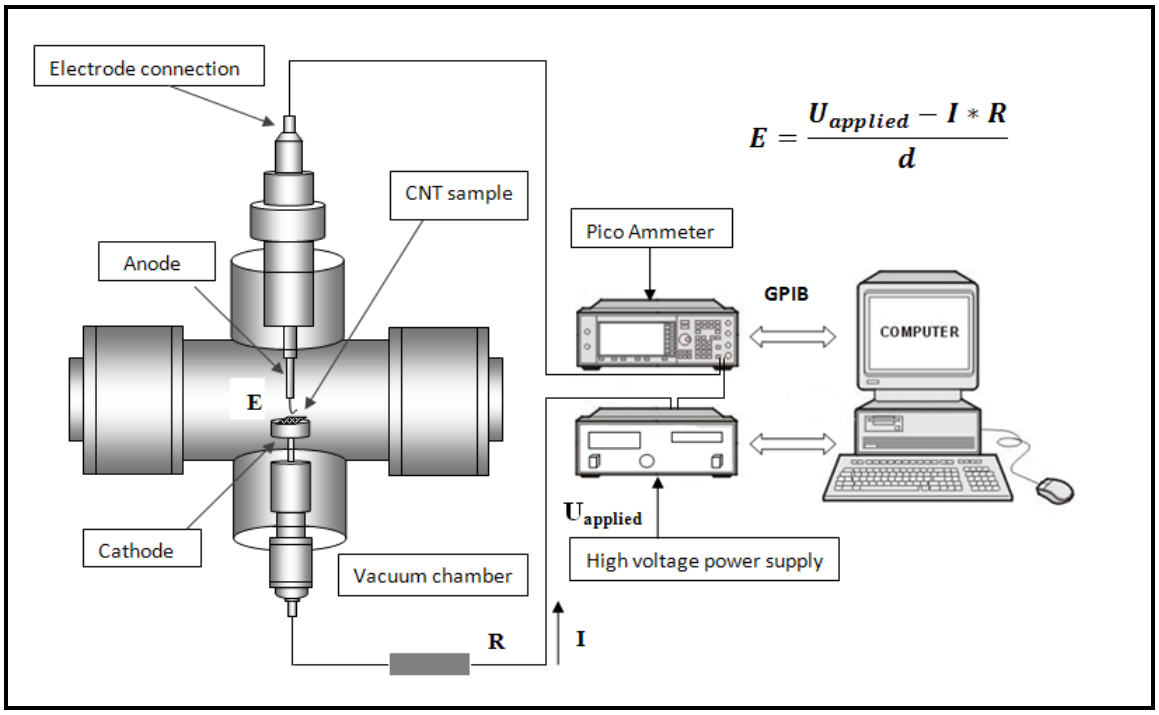

(b)

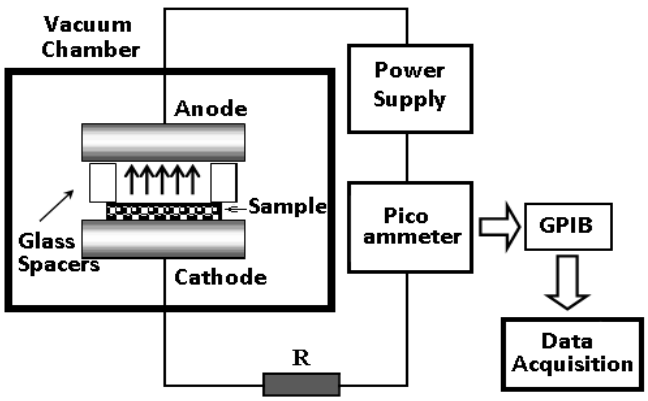

Figure 4.5 Field emission measurement setup (a) Schematic (b) Block diagram

Computer controlled DC voltage source and pico-ammeter were used to measure the *I–V* characteristics. A digital DC power supply (Stanford Research Systems PS235) is used to apply a voltage between the anode and cathode. A Keithley 485 pico-ammeter is used to measure the emission current. In our

experiments a cylindrical rod acting as anode with known area of 0.031415cm^2 emitting surface is exposed to the CNT sample in order to limit the total current flow within the range of the power supply. The measured electron emission current was divided by the area of the cathode to calculate the field emission current density.

Initially the chamber is evacuated to the vacuum level until the pressure reaches to ~$5x10^{-7}$ Torr and the field emission characteristics at vacuum are acquired. Each time the voltage applied from 0 to 1200V with variable voltage steps depending on the data resolution required in the curve. The field emission curves in vacuum are considered as the base data. Further field emission experiments were carried out in Helium and Dry air respectively at different pressures ranging from $5x10^{-7}$ to $20x10^{-3}$ Torr. The pressure of the chamber is varied by inputting the relevant gas each time through gas valves. The field emission data is acquired using the data acquisition system as voltages with respective currents. We use the field emission curves as a function of current density and electric field to figure out the turn-on electric field densities in each case are noted using these plots.

4.3 F-N curves of MWCNTs in vacuum ambience

As described by the field emission definition, the emission of electrons from the surface of a condensed phase into another phase, usually a vacuum, under the action of high (0.3-0.6 V/A) electrostatic fields [62]. As I have introduced in chapter 3, the field emission is a quantum mechanical phenomenon. In vacuum ambience, the energy which makes the electrons tunneling through the barrier of CNTs surface should all came from the extra high voltage between the anode and cathode. Then it should follow the Fowler-Nordheim equation and get a straight line in the F-N coordinate. While from our experiment result, we got a bundle of non-linear lines instead of straight lines as we have expected. It may due to the Fowler-Nordheim

equation only base on the conductive material especially metal and the plain topographic. However, in our case, the MWCNTs are a kind of semiconductor, and its topographic is much more complicated than the plain metal. So we need a new model to explain the field emission from the MWCNTs. Then we forced that we can easily make use of the field enhancement factor β to explain some of our result in order to get the best synthesis condition of the MWCNTs which can get a good field emission result. First, we analyze the field emission result which came from the MWCNTs are grown on pure silicon. We compare the field emission properties from the MWCNTs with varied growth and sputtering time. Then we also analyze the field emission result from the MWCNTs are grown on silicon substrates with silicon dioxide and titanium underlying layer in vacuum ambiance.

4.3.1 Compare the different growth times of MWCNTs on pure silicon

First, the field emission data is recorded in vacuum pressure of 10^{-7} Torr first and then the FN plots are generated using Fowler-Nordheim Equation 3.3. Comparison of the FN plots of each sample in vacuum condition is shown in Figure 4.6. As expected, the FN plots for all samples exhibit some form of non-linearity, and the location of the "knee" varies with varying growth condition. In Figure 4.6, the low field and high field regions are labeled. From the FN plots, we have fitted a straight line to the data and determined two distinctive slopes, namely k_1 (for high field) and k_2 (for low field) and the "knee" location for each curve. For each slope, a field enhancement factor is calculated and tabulated as shown in Table 4.1 for each set of samples. As the growth time increases, the knee becomes more pronounced reaching the highest value for the sample with 240 min growth time for both 5 min and 10 min catalysis sputtering times. The data also shows that the field enhancement factor increased with the growth time increase of each sample tested in

vacuum. Our samples are randomly oriented CNTs and, if the tube lengths are too long (in the case of 240 min growth time) they may get entangled. However, this random distribution of the tubes doesn't seem to have much effect on the field enhancement factor in vacuum. The samples with 10 min growth time seem to have the poorest field emission and field enhancement factors. This is understood, because if the tube density at this short growth time is not very high; therefore the number of emitters contributing to the electron emission process is low. Considering the data, we conclude that the optimal fabrication condition for a sample with high field enhancement factor and low turn-on field is 120 min growth time for either sputtering time. On the other hand, the samples with 10 min and 5 min sputtering time in vacuum perform different field emission result.

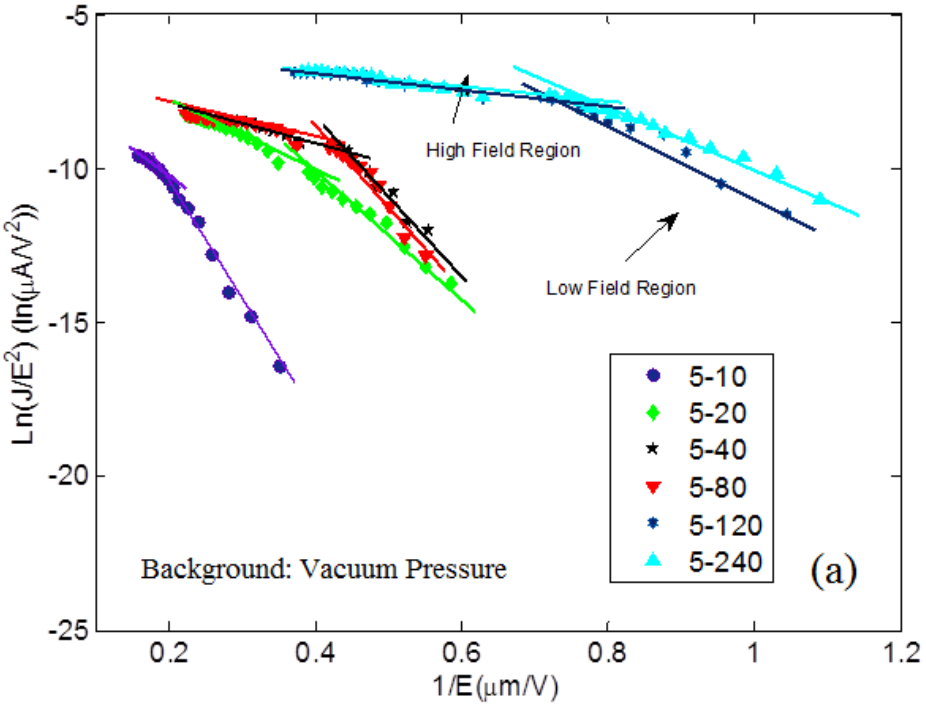

(a)

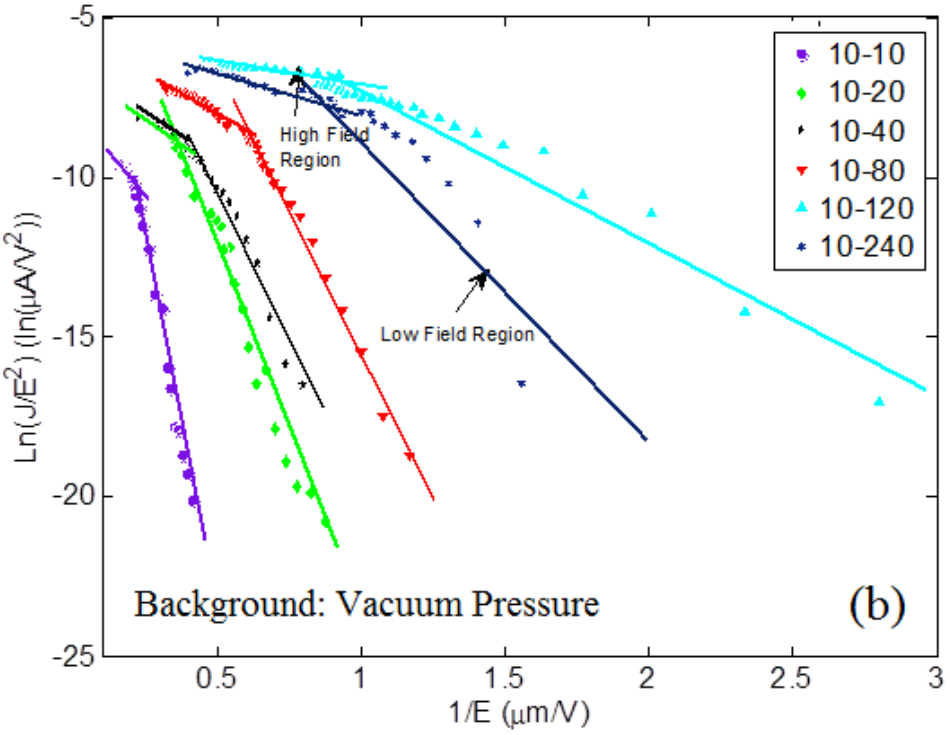

(b)

Figure 4.6 FN plots with 5 min (a) and 10 min (b) sputtering time and various growth times

Table 4.1: Field Emission and Enhancement of the samples with 5 min sputtering time in vacuum pressure of 10^{-7} Torr

Sample Name	Slope Coefficient		Field Enhancement factor		"knee" location (V/μm)	turn on field (V/μm)
	k_1	k_2	β_1	β_2		
5-10	-25.68	-40.63	2539	1604.7	4.45	1.71
5-20	-9.841	-23.24	6625	2805.5	2.99	1.16
5-40	-4.908	-29.86	13284	2183.5	2.22	1.07
5-80	-6.961	-28.05	9366	2324.4	2.11	1.07
5-120	-3.235	-13.79	20154	4728	1.25	0.57
5-240	-2.707	-12.36	24085	5275	1.31	0.53

Table 4.2: Field Emission and enhancement of samples with 10 min sputtering time in vacuum pressure of 10^{-7} Torr

Sample Name	Slope Coefficient		Field Enhancement factor		"knee" location (V/μm)	turn on field (V/μm)
	k_1	k_2	β_1	β_2		
10-10	-13.61	-50.75	4791	1285	4.75	1.43
10-20	-5.1888	-64.32	12567	1014	2.57	1.04
10-40	-4.82	-19.31	13527	3376	2.24	1
10-80	-5.154	-17.77	12650	3669	1.69	0.57
10-120	-1.813	-5.625	35962	11591	0.88	0.57
10-240	-1.965	-6.487	33180	10051	1.11	0.43

4.3.2 Compare the different sputtering times of MWCNTs on pure silicon

From the last section, we notice not only the growth time but also another important factor during the fabrication process may affect the field emission result. So, for the same growth time, we compare the FN curves with varied catalyst sputtering times before we grow the tube. Figure 4.7 (a) and Figure 4.7 (b) show us the FN plots from 5 min and 10 min sputtering time tubes in vacuum ambiance with 20 min and 80 min growth time separately. And Table 4.3 gives us the slope coefficient and corresponding field enhancement factors for each fitted lines.

Table 4.3 Field emission and enhancement of samples with 10 min, 5 min sputtering times and 20 min and 80 min growth times in vacuum pressure of 10^{-7} Torr

Sample name (test in vacuum)	Slope Coefficient		Field Enhancement factor		"knee" location (V/μm)	turn on field (V/μm)
	k_1	k_2	β_1	β_2		
5-80	-6.961	-28.05	9366	2324.4	2.11	1.07
10-80	-3.727	-16.43	17494	3968.3	2.069	0.57
5-20	-8.402	-23.06	7759.9	2827.4	2.69	1.03
10-20	-5.188	-64.32	12567	2671	2.85	1.04

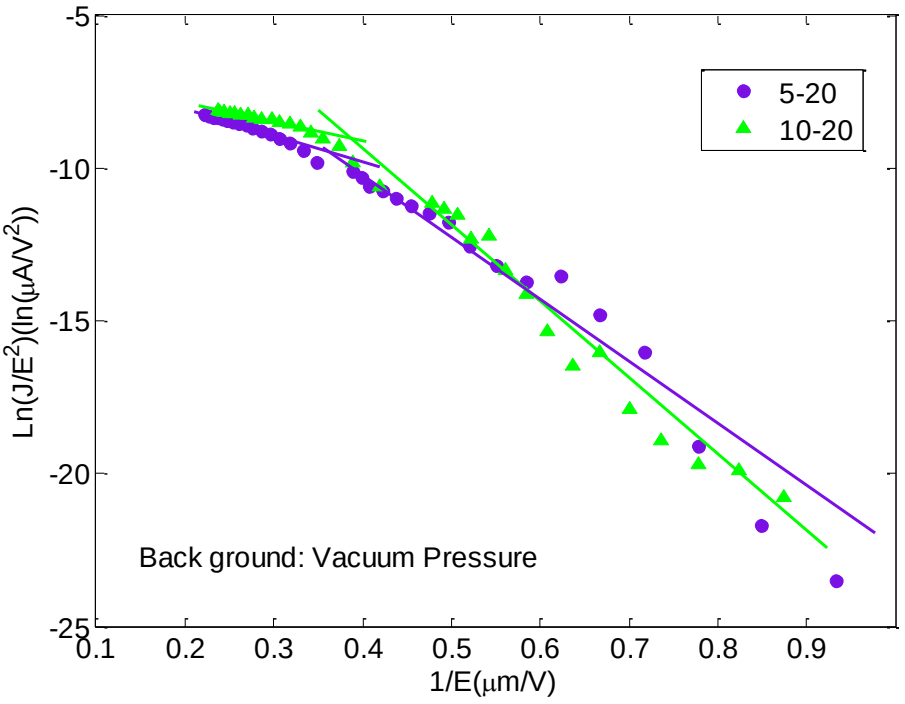

(a)

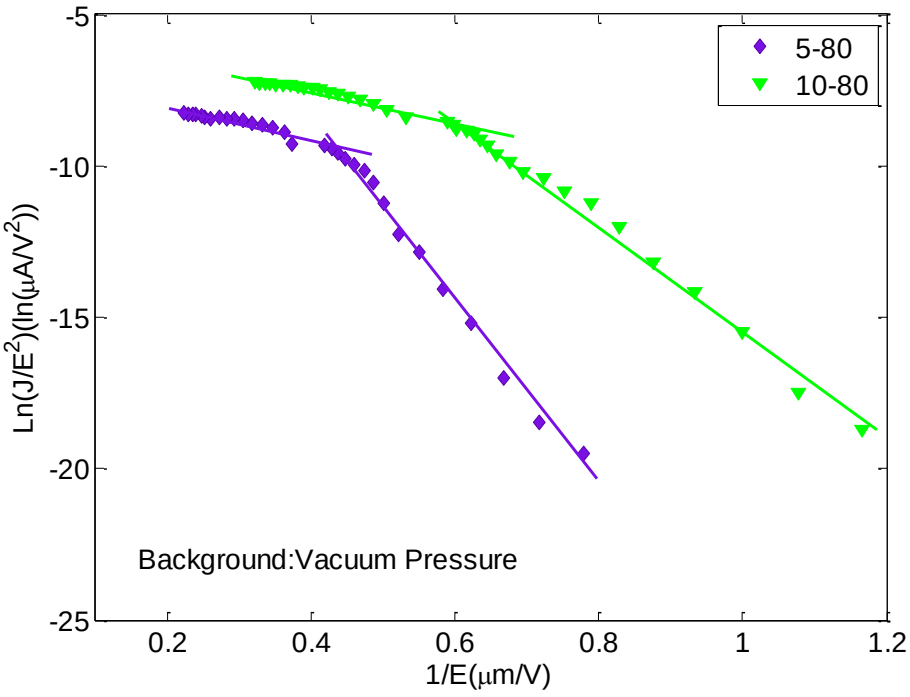

(b)

Fig 4.7 FN plots with 20 min (a) and 80 min (b) growth time and various sputtering time under vacuum field emission test ambiance.

From Table 4.3 we can easily found that the sputtering time increasing accompanied with the increasing of the field enhancement factor β in both field emission processes. The thickness of the catalyst is decided by the sputtering time. So the longer sputtering time means the thicker catalyst layer here. The iron particle which located on the top of the tube may affect the field emission performance. The phenomenon that thicker catalyst layer will lead to better field emission performance can be explained by the existence of these nano-particles will effectively increase the aspect ratio lead to larger field enhancement factor. Furthermore the nano size particle in the tubes may decrease the work function of the CNTs which will also lead much better field emission performance.

While we also notice that the length of the tubes has more great effect on the field emission performance than the sputtering time. When the tube is long enough (grown time is over 40 min), the field enhancement factor of the tubes which has been experience 10 min sputtering process is much larger than the tubes with 5 min sputtering process. While for the short tubes (grown time is 20 min), the field enhancement factor does not change greatly but still shown the same trend. The change of the 'knee' location on the FN curves and the turn on field between the 5 min and 10 min sputtering time prove longer sputtering time, especially when the tubes are long enough, indeed lead to a better field emission performance than the shorter sputtering time.

4.3.3 Compare the different sputtering times of MWCNTs on silicon dioxide

In order to verify the barrier between the silicon substrate and the CNTs indeed affect the field emission result, we grow the CNTs on silicon dioxide layer which sputtering on the pure silicon substrate first. Then measure the field emission

characterizes and plot the Field emission curve (applied electric field vs. current density) and the FN curve (1/E vs. Ln (J/V^2)) separately. All the samples grown on the silicon dioxide have the same growth time (20 min) and field emission tests in this section were all taken in high vacuum condition (1×10^{-7} Torr). The thickness of the silicon dioxide layer is about 0.6μm [27].

By compared of the turn on field and the field enhancement factor β, the CNTs which grown on the silicon dioxide layer have worse field emission performance than the CNTs which grown on the pure silicon (higher turn on field and smaller field enhancement factor). That phenomenon can be explained easily by the barrier model as we have described before. As the silicon dioxide layer was added between the CNTs and the pure silicon substrate, the barriers between the CNTs and substrate become two instead of only one which will lead the electrons more hard to tunnel though.

I compare the FN curves with varied sputtering time before we grow the tube on the silicon dioxide layer. Figure 4.8 (a) and Figure 4.8 (b) show us the field emission curves and FN plots from 5 min and 10 min sputtering time tubes in vacuum ambiance with 20 min growth time separately. And Table 4.4 gives us the slope coefficient and corresponding field enhancement factors for each fitted lines.

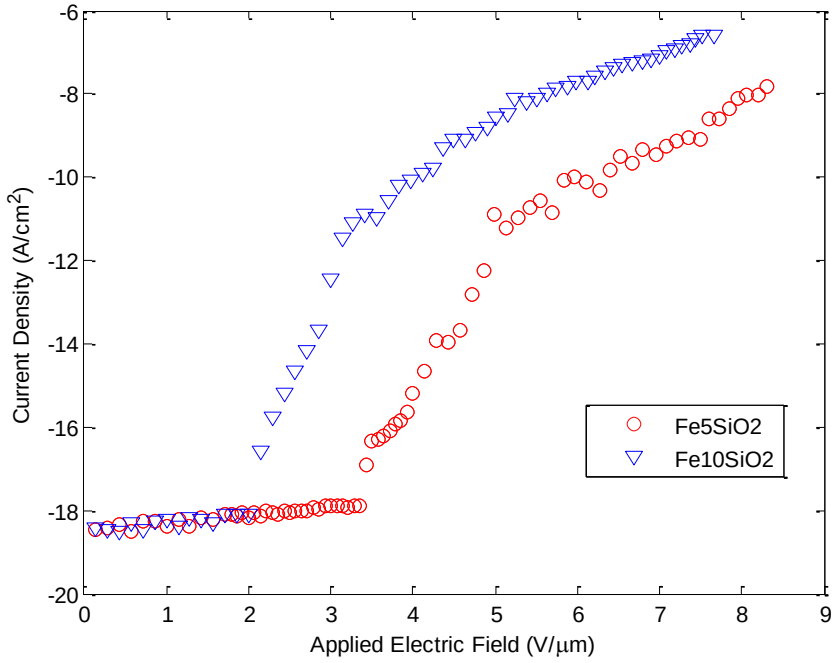

(a)

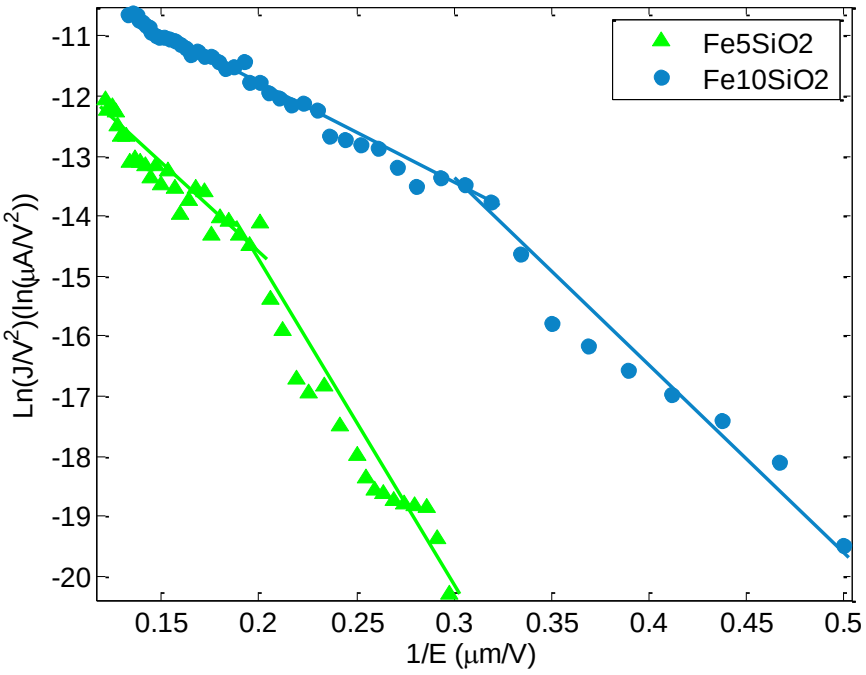

(b)

Fig 4.8 Field Emission Curves (a) and FN plots (b) on SiO_2 with 20 min growth time and various sputtering time under vacuum field emission test ambiance.

Table 4.4 field emission enhancement factors of samples with 10 min, 5 min sputtering times and 20 min growth times in vacuum pressure of 10^{-7} Torr

Sample Name	Slope Coefficient		Field Enhancement factor		"knee" location (V/μm)	turn on field (V/μm)
	k_1	k_2	β_1	β_2		
$Fe5SiO_2$	-29.67	-49.38	2197	1320	5.134	3.428
$Fe10SiO_2$	-17.12	-27.38	3808	2381	3.275	2.143

Then I can find that the field enhancement factor β increased greatly with the sputtering time increase. That pheromone means the longer sputtering time indeed increase the surface roughness level and lead to the increasing of β which finally result the turn on field become decreased. Thus we can get the conclusion that the CNTs on the silicon substrate with silicon dioxide underlying layer have the same trend as the CNTs on the pure silicon substrate which is the longer sputtering time will lead much better field emission performance.

4.3.4 Compare the different sputtering times of MWCNTs on Ti underlying layer

We also test the field emission characterizes of CNTs which grown on the Silicon substrate with Ti underlying layer. The CNTs samples with Ti underlying layer all prepared with 20 min grown time and test field emission characterizes under high vacuum ambiance (1×10^{-7} Torr). The thickness of the Ti underlying layer is approximate 0.6μ [27]. Figure 4.9 (a) and Figure 4.9 (b) show us the field emission curves and FN plots from 5 min and 10 min sputtering time tubes in vacuum ambiance with 20 min growth time separately. And Table 4.5 gives us the slope coefficient and corresponding field enhancement factors for each fitted lines.

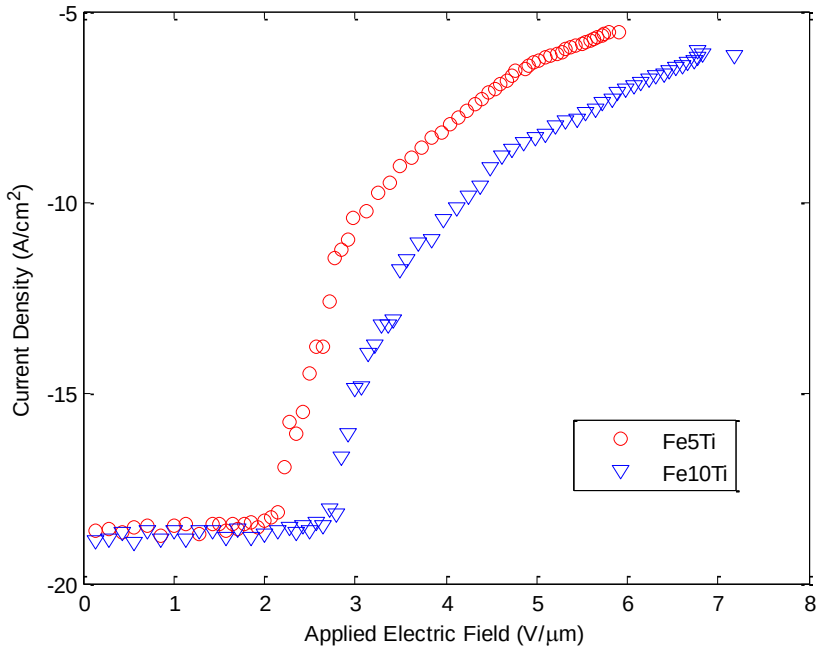

(a)

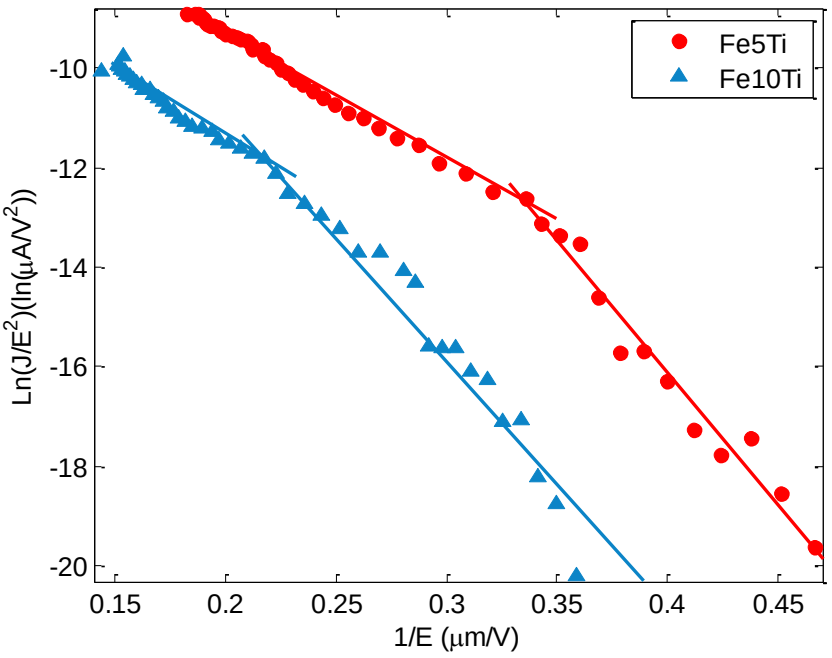

(b)

Fig 4.9 Field Emission Curves (a) and FN plots (b) on Ti underlying layer with 20 min growth time and various sputtering time under vacuum field emission test ambiance.

First, we compare the turn on field of the CNTs grown on pure silicon with the one grown on Ti underlying layer. The result shown the turn on field of the samples which grown on Ti underlying layer are increase a lot by compared to the samples with the same growth and sputtering time on pure silicon. That verified the extra barrier between the silicon substrate and the CNTs block the electron tunneling process and lead to lower turn on field.

In J. Zhang ‘s paper they have been introduced they can hardly find a ‘knee’ on the CNTs on Ti [55]. They explained it by carbon is reactive to Ti and formed conductive titanium carbide (TiC) interlayer rather than oxide. While From the FN plots as shown on Fig 4.9 (b) we can find obvious ‘knee’ on both of the FN curves. That may be caused by the thickness of the Ti film. The thickness of Ti layer on our samples is approximate 0.6μm which is much thicker than Zhang’s sample with 100 nm Ti film. Then we can get the conclusion that although carbon is reactive to Ti, the thicker Ti film still will lead to a wide barrier between the CNTs and the Ti layer which will eventually block the tunneling process.

Different from the sample which grown CNTs on pure silicon and silicon dioxide. The CNTs samples which grown on Ti layer exhibited lower field enhancement factor with increased sputtering time. Longer sputtering time didn’t result more roughness surface which will lead to better field emission performance in this case. Conversely, longer sputtering time result a thick iron layer which lay on the Ti film, then the iron will not work as a catalyst and may result another layer make another barrier between CNTs and Ti which lead worse turn on field. While for the sample which grown on silicon dioxide layer with 10 min sputtering time and 20 min growth time even have more lower turn on field than the sample which grown on Ti layer under the same sputtering and grown time. So our conclusion is the roughness of

the surface will greatly affect the field emission performance and the time of sputtering catalyst is a critical step for synthesis CNTs with good field emission performance. The unsuitable catalyst layer thickness on the underlying layer may lead the conductive layer have even worse performance during the field emission process than the isolated layer.

Table 4.5 field emission enhancement factors of samples on Ti underlying layer with 10 min, 5 min sputtering times and 20 min growth times in vacuum pressure of 10^{-7} Torr

Sample Name	Slope Coefficient		Field Enhancement factor		"knee" location (V/μm)	turn on field (V/μm)
	k_1	k_2	β_1	β_2		
Fe5Ti	-23.58	-51.74	2765	1260	3.12	2.214
Fe10Ti	-30.02	-66.56	2172	979.5	3.49	2.857

4.4 F-N curves of MWCNTs in Helium ambience:

Field emission concept is only described the situation that the electrons are extract from the conductive material surface to vacuum. While in real application, we can hardly get high vacuum condition. In the partial pressure condition, the atom in the background gas will affect the efficient of the electrons get the anode. Furthermore the effective length and the effective density of the CNTs participate in the field emission process will also be affect by the background gas. All of that will affect the current we collected from the field emission process. In our experiment, we fill our chamber with partial pressure Helium gas.

In order to know how the varied pressures affect our field emission result, we compare the CNTs with different growth time and sputtering time in 20mTorr

pressure Helium ambience by plot FN curve and give the result some explanations by hiring our module. Then we varied the pressures to analyze how the gas pressure affects the field emission result. By compare the field emission result, we found that the partial pressure indeed reduce the current that we collected than in vacuum ambiance. While we also found the optimal synthesis condition of CNTs which will give us best field emission result are different from the conditions we have got from the vacuum test ambiance.

4.4.1 Compare the different growth times

As test process in vacuum, the field emission data now is collected in partial pressure of $20x10^{-3}$ Torr helium background gas. Then, from the field emission data, the FN plots are generated and comparison is made. Although both sets of samples are tested, only the results of the samples with 5 min sputtering time are presented here. As expected the F-N plots exhibit some form of non-linearity for this case also, and the location of the "knee" varies with varying growth condition. Figure 4.10 shows the FN plots of the samples and the Table 4.6 summarizes the slope and field enhancement factors for both the low and high field regions, along with the "knee" location and the turn-on-field.

From Table 4.6, we note that for the same sputtering time the knee shifts to the low electrical field as the growth time increases indicating that the growth time and knee location are inversely proportional. This is also true for the turn-on-field, where the longer growth time results in lower turn on field [60]. Also, the field enhancement factor, β, increases greatly with the growth time increase. This can be explained: when the growth time increases the carbon nanotubes grow longer, so the aspect ratio of the tubes increases. Increased aspect ratio results in an increased field enhancement factor β.

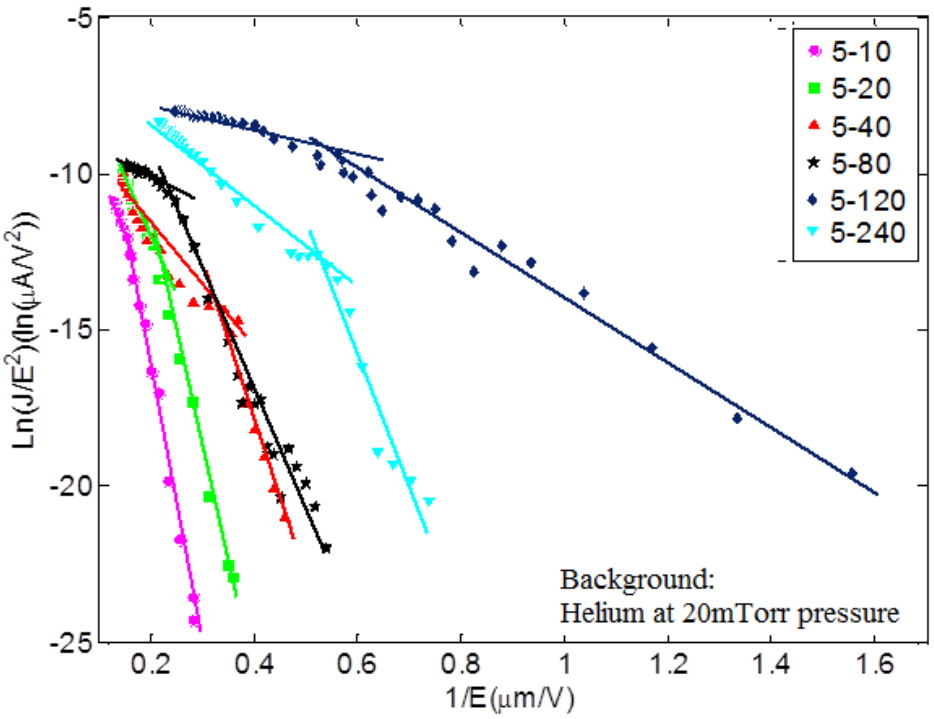

Fig 4.10 FN plots of the samples under 20mTorr Helium field emission test ambiance.

Table 4.6 Field emission data of samples with 5 min sputtering time and various growth times tested in Helium at 20mTorr pressure.

Sample Name	Slope Coefficient		Field Enhancement factor		"knee" location (V/μm)	turn on field (V/μm)
	k_1	k_2	β_1	β_2		
He 5-10	-45.64	-92.49	1429	704.9	6.32	3.43
He 5-20	-44.29	-64.32	1472	1013.7	5.48	2.57
He 5-40	-25.13	-52.24	2594	1248.1	5.52	2.07
He 5-80	-9.89	-34.08	6592	1913.1	4.04	1.78
He 5-120	-2.928	-9.245	22264	7052.3	2.49	1.36
He 5-240	-14.08	-36.56	4631	1783.3	2.14	1.21

4.4.2 Compare the different sputtering times

In 20m Torr Helium background gas test ambiance, we also compare the FN plots of the CNTs with different sputtering time as shown in Fig 4.11 (a) and Fig 4.11 (b). From table 4.7 we found the similar phenomena as in the vacuum test ambiance that the sputtering time increasing accompanied with the increasing of the field enhancement factor β in both field emission processes. That means the thickness of the catalyst layer also affect the field emission performance.

By compared the FN plots of CNTs which have the same grown condition but different test ambiance, we notice that the field emission performance in vacuum is better than in 20m Torr helium background gas test ambiance. While the tubes with longer sputtering time have more field enhancements factor derivation between the tubes test in vacuum and in 20m Torr Helium test ambiance than the derivation of the tubes with shorter sputtering time. Consequently, the longer sputtering time can make the tubes have better field emission performance in high pressure test ambiance.

We also found the length of the tubes has more great effect on the field emission performance than the sputtering time as the result in vacuum test ambiance. When the CNTs tubes are short no matter the field emission test were carried on in vacuum or in partial pressure test environment the iron catalyst particles in the tubes are located near the surface, so just have limited effect on changing the field emission performance. However, if CNTs tubes are long enough then, when the field emission test process carried on partial pressure ambience the background gas may blow the tiny tubes up which may result the iron particle improve the FE performance. Take the sample called 10-80 as an example, the field enhancement factor for this sample which test field emission characteristic under the partial pressure condition have better performance than under the vacuum test environment.

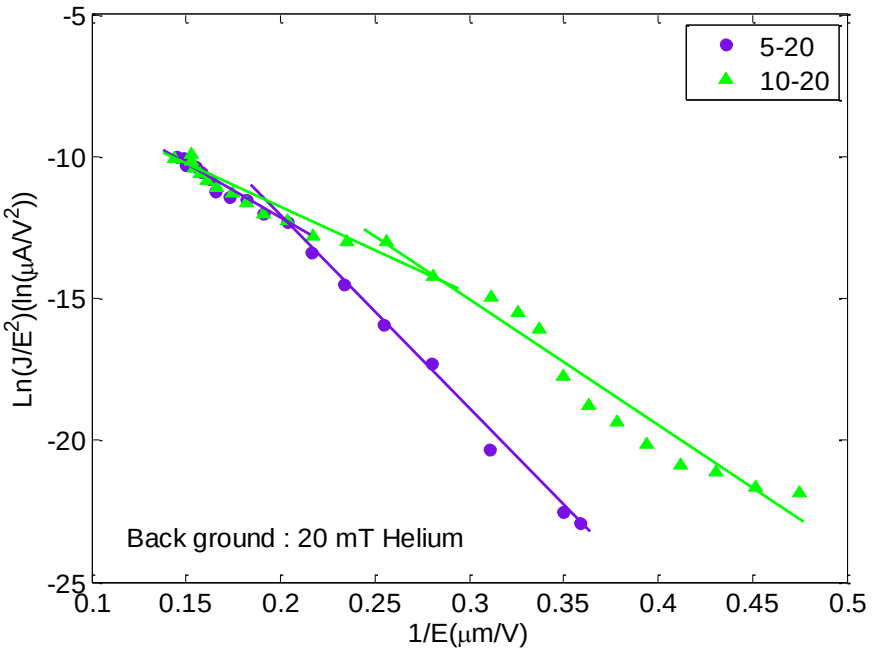

(a)

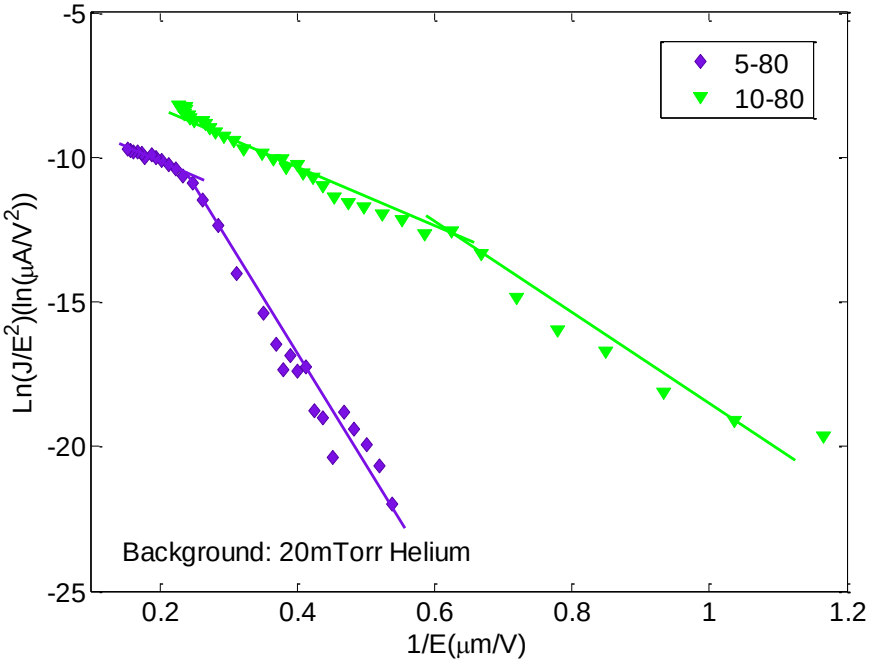

(b)

Fig 4.11 FN plots with 20 min (a) and 80 min (b) growth time and various sputtering time under 20m Torr Helium field emission test ambiance

Table 4.7 Field emission and enhancement of samples with 10 min, 5 min sputtering times and 20 min and 80 min growth times in Helium at 20mTorr pressure

Sample name	Slope Coefficient		Field Enhancement factor		"knee" location (V/μm)	Turn on field (V/μm)
	k_1	k_2	β_1	β_2		
He 5-80	-11.4	-35.38	5719	1842.8	4.137	1.78
He 10-80	-9.802	-13.41	6652	4862	2.482	0.86
He 5-20	-44.29	-64.32	1472.1	1013.7	5.52	2.69
He 10-20	-36.1	-45.47	1806	1433.9	3.93	2.57

4.4.3 Compare the different pressure

For examinate the effects of pressure on the fied enhancement factor, the samples are tested in varying backgroud pressure from vacuum to 20mTorr with an order of magnitude increase. Then, the same data analysis is conducted and FN plots are plotted. In Figure 4.12 (a) and (b), we show the data of the 5-20 and 5-80 (the sample with 5 min sputtering time and 20 min, 80 min growth times). In Table 4.8, the data collected in vacuum is also included for comparison. From this data we observe that as the pressure decreases the location of the knee and the turn on field shift to the low electrical field which means the turn on field decreases. Furthermore as the pressure decreases the field enhancement factor β increases. In the vacuum condition, the field enhancement factor is high as expected. As the pressure increases, the electrons extracted from CNTs will interact with the background gas while on their way to the anode (the collector). Therefore the field enhancement factor decreases as the gas pressure increases. Furthermore, the quantum tunneling process is only defined in vacuum for a field emission process. In higher pressure, the “vacuum-material” potential barrier deformation is not the same, and the electron

emission process is expected to be less efficient, as the electrons cannot tunnel through the potential barrier effectively.

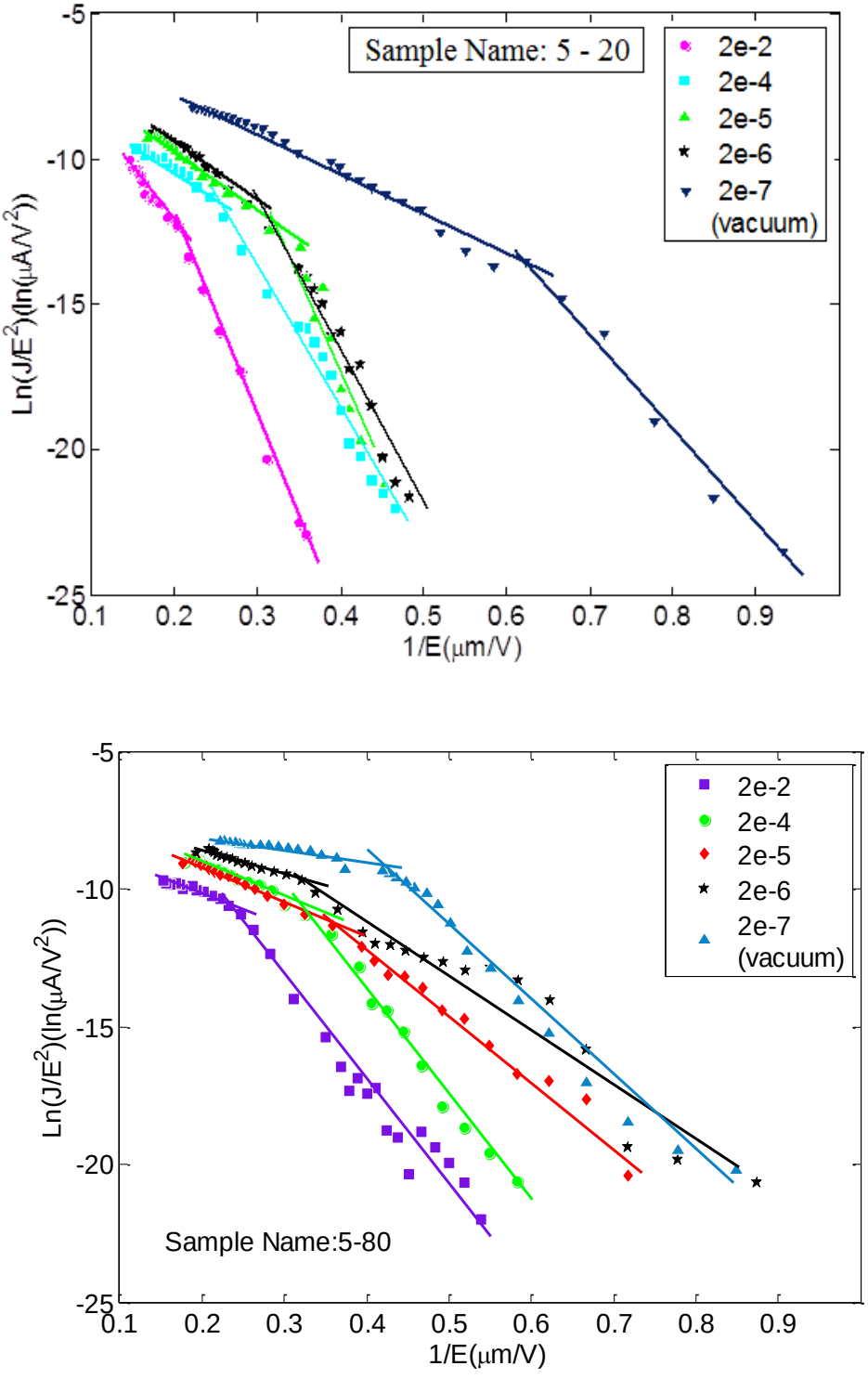

Fig 4.12: FN plots with 20 min (a) and 80 min (b) growth time and 5 min sputtering time under various helium background gas pressures

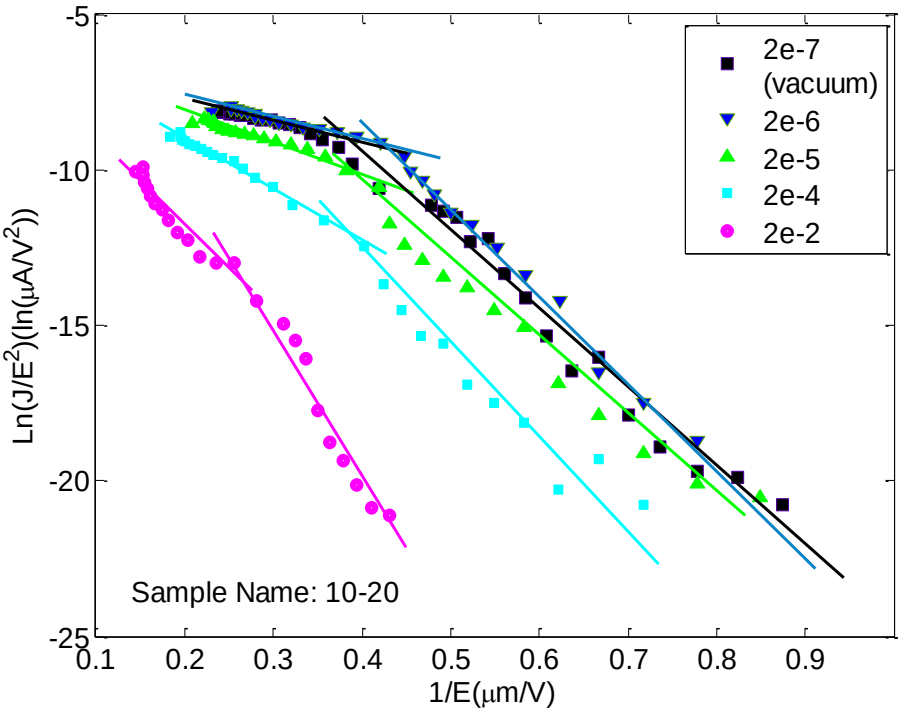

(a)

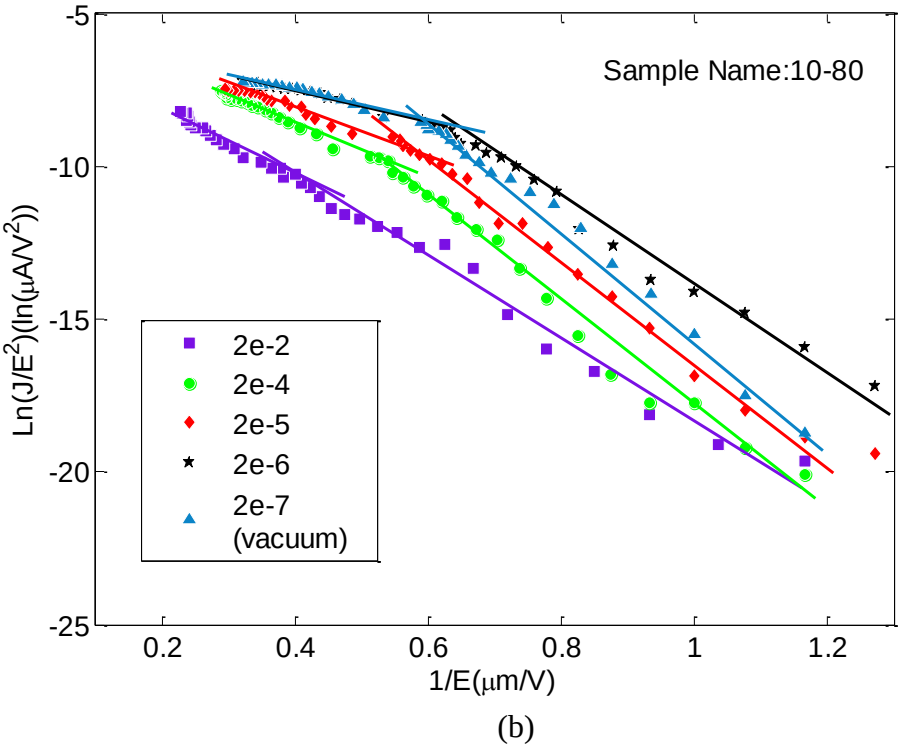

(b)

Fig 4.13 FN plots with 20 min (a) and 80 min (b) growth time and 10 min sputtering time under various helium background gas pressures

Table 4.8 Field emission and enhancement of samples with 5 min sputtering times and 20 min growth times in various Helium pressures.

Sample name	Slope Coefficient		Field Enhancement factor		"knee" location	turn on field (V/μm)
	k_1	k_2	β_1	β_2	(V/μm)	
He 5-20 2e-2	-44.29	-64.32	1472.1	1013.7	800	390
He 5-20 2e-4	-26.11	-48.07	2497.1	1356.3	650	300
He 5-20 2e-5	-33.76	-78.6	1931.2	829.5	450	300
He 5-20 2e-6	-40.01	-76.81	1629.6	848.8	340	290
vacuum 5-20	-8.402	-23.06	7759.9	2827.4	390	150

Table 4.9 Field emission and enhancement of samples with 10 min sputtering times and 20 min growth times in various Helium pressures.

Sample name	Slope Coefficient		Field Enhancement factor		"knee" location	turn on field (V/μm) [Ramesh]
	k_1	k_2	β_1	β_2	(V/μm)	
He 10-20 2e-2	-36.1	-45.47	1806	1433.9	3.93	2.57
He 10-20 2e-4	-16.21	-25.7	4022	2536.9	2.5	1.54
He 10-20 2e-5	-8.56	-22.08	7617	2952.8	2.5	1.18
He 10-20 2e-6	-5.94	-28.05	10976	2324.4	2.5	1.08
Vacuum 10-20	-5.188	-64.32	12567	2671	2.85	1.04

Table 4.10 Field emission and enhancement of samples with 5 min sputtering times and 80 min growth times in various Helium pressures.

Sample name	Slope Coefficient		Field Enhancement factor		"knee" location	turn on field (V/μm)
	k_1	k_2	β_1	β_2	(V/μm)	
5-80 2e-2	-11.4	-35.38	5719	1842.8	4.137	1.78
5-80 2e-4	-13.56	-40.96	4808	1591.8	4.137	1.5
5-80 2e-5	-13.76	-20.92	4738	3116.6	2.379	1.4
5-80 2e-6	-10.03	-20.32	6500	3208.6	3.103	1.14
Vacuum 5-80	-6.961	-28.05	9366	2324.4	2.172	1.07

Table 4.11 Field emission and enhancement of samples with 10 min sputtering times and 80 min growth times in various Helium pressures.

Sample Name	Slope Coefficient		Field Enhancement factor		"knee" location (V/μm)	turn on field (V/μm)
	k_1	k_2	β_1	β_2		
10-80 2e-2	-9.802	-13.41	6652	4862.0	1.91	1.178
10-80 2e-4	-9.272	-17.33	7032	3762.2	1.85	1.14
10-80 2e-5	-7.839	-15.71	8317	4150.1	2.06	0.99
10-80 2e-6	-4.947	-13.38	13179	4872.9	1.67	0.86
Vacuum 10-80	-5.154	-17.77	12650	3669.0	1.52	0.99

4.5 F-N curves of MWCNTs in dry air ambience:

In this part, our field emission test process was carried on the dry air ambience which is more close to the real application case. As we have said previous, in partial pressure condition, the atom in the gas will affect the field emission result. This time we fill our chamber with partial pressure dry air as background gas.

We plot F-N curves for different synthesis conditions and different pressure conditions. Then we compare the CNTs with different growth time and sputtering time in partial pressure dry air ambience. Then we varied the pressures to analyze how the gas pressure affects the field emission result. By compare the field emission result, we found that the partial pressure indeed reduce the current that we collected than in vacuum ambiance as we expect and the optimal synthesis condition of CNTs which will give us best field emission result are different from the conditions we have got from the vacuum test ambiance or in Helium background gas test ambience. What more interested here is we can hardly find a 'knee' on the FN plot when the background gas is dry air. There must be some oxygen molecule which can absorb electrons that extract from CNTs. Then the space charge effect will have little effect on the FE which takes under the dry air ambience.

4.5.1 Compare the different growth times

As this step, the field emission data is recorded in partial pressure of 20×10^{-3} Torr dry air background gas. Then, I plot the field emission data in the F-N coordinate to generate the F-N curves. They are not show the non-linearity as the curves which we get from the Helium and vacuum test environment. Although both sets of samples are tested, only the results of the samples with 5 min sputtering time are presented here. We can fit our experiment data by a bundle of straight lines as shown in Figure 4.14 and the Table 4.12 summarizes the slope and field enhancement

factors and the turn on field for these lines. From Table 4.12, we note that under the same field emission test ambience (20 mTorr), the field enhancement factor β is increasing and the turn-on-field decreasing greatly with the grown time increasing [60]. What more interested is when the tubes are short (grown time 10 min 20 min 40 min and 80 min), the field enhancement factor was not greatly changed by the background pressure. While the long tubes (grown time are 120 min and 240 min), the field enhancement factor β is increase greatly with the background pressure decrease.

This can be explained: when the growth time increases the carbon nanotubes grow longer, so the aspect ratio of the tubes increases results in an increased field enhancement factor β as in vacuum ambiance. And some ionized atom in dry air may combined with some of the electrons which were extract from the CNTs carpet, which lead the result that we cannot get the saturation point of the field emission.

Table 4.12 Field emission and enhancement of samples with 5 min sputtering times and various growth times in 20mTorr dry air background gas.

Sample name (test in 20m Torr)	Slope Coefficient	Field Enhancement factor	turn on field (V/μm) [Ramesh]
	k_1	β_1	
5-10	-78.71	828	3.75
5-20	-52.07	1252	2.93
5-40	-46.32	1408	2.5
5-80	-35.2	1852	2.5
5-120	-22.55	2891	1.57
5-240	-16.67	3911	1.28

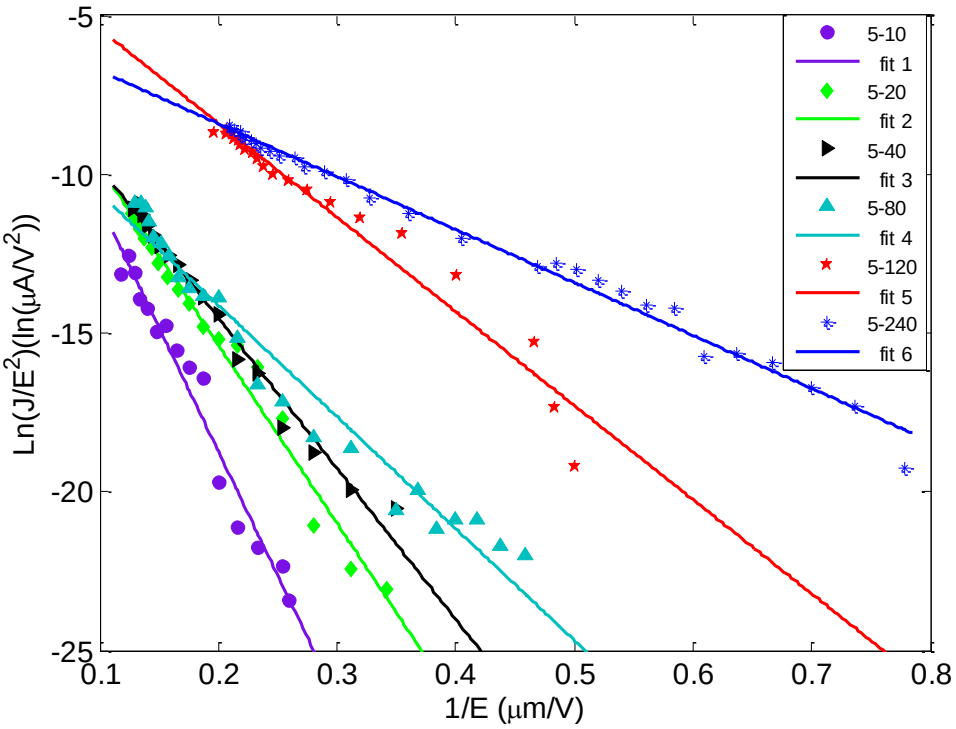

Fig 4.14: FN plots with 5 min sputtering time and various growth time under 20m Torr dry air field emission test background gas

4.5.2 Compare the different sputtering times

In 20m Torr dry air ambiance, we also compare the FN plots from the CNTs with different sputtering time as shown in Fig 4.15(a) and (b). From Table 4.13 we found the similar phenomena as in the 20m Torr helium test ambiance that the sputtering time increasing accompanied with the increasing of the field enhancement factor β. And the turn on field are also shown us the same trend. That means no matter the field emission test ambiance is, the longer catalyst sputtering time of CNTs grown on pure silicon substrate can always improve the field enhancement factor.

Although under the dry air test condition, the current does not get saturation as under vacuum and helium test condition. The field enhancement factor β here does not change much compare with the β in helium test environment but a little bit higher than in helium test condition. So we can get the conclusion here, under the same

pressure condition we can almost get the same field emission enhancement factor no matter the species of the background gas.

Table 4.13 Field emission and enhancement of samples with 10 min, 5 min sputtering times and 20 min and 80 min growth times in 20mTorr dry air background gas.

Sample name (test in vacuum)	Slope Coefficient	Field Enhancement factor	turn on field (V/μm)
	k_1	β_1	
5-20	-52.07	1252	2.93
10-20	-32.9	1981.7	3
5-80	-35.2	1852.2	2.5
10-80	-15.91	4098	1.29

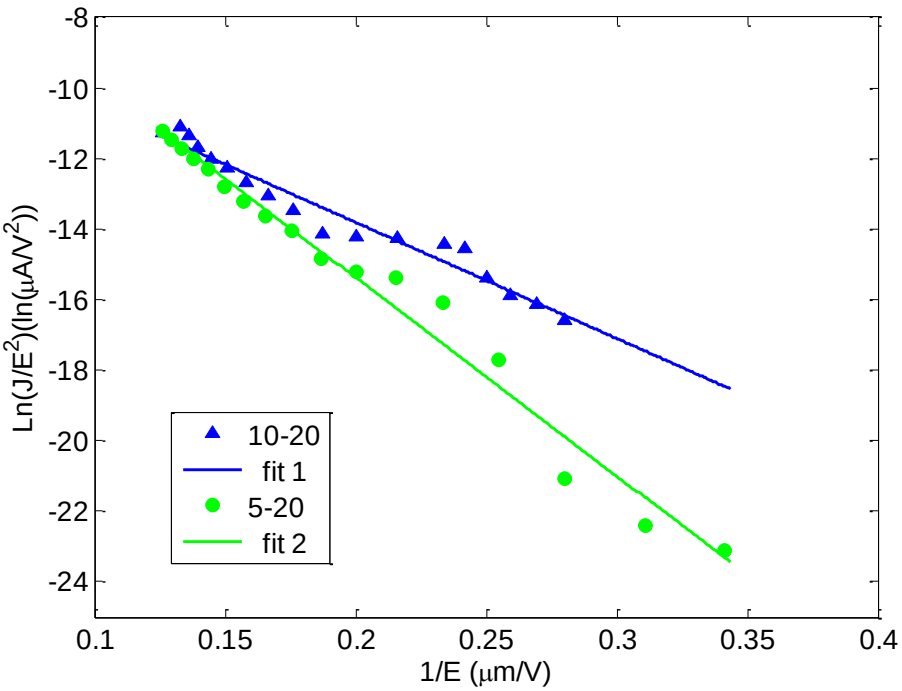

(a)

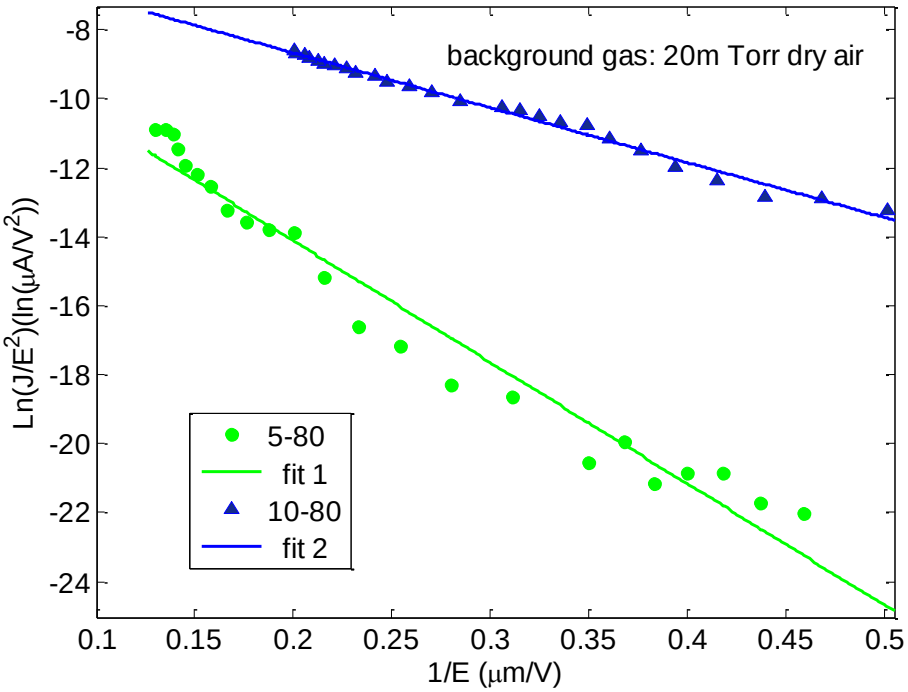

(b)

Fig 4.15: FN plots with 20 min (a) and 80 min (b) growth time and various sputtering time under 20m Torr dry air background gas

4.5.3 Compare the different pressures

In dry air back ground gas ambiance, for examine the effects of pressure on the fied enhancement factor, the samples are tested in varying backgroud pressure from vaccum to 20mTorr with an order of magnitude increase like we have done in helium back ground gas ambiance. Then, the same data analysis is conducted and FN plots are plotted. In Figure 4.15, we show the data of only the 5-20 (the sample with 5 min sputtering time and 20 min growth time). In Table 4.14, the data collected in vacuum is also included for comparison. As we have discussed before, the FN plot not shown us any apparetlly 'knee' like in the helium gas test environment. However, we still found that as the pressure decreases the field enhancement factor β increases. At the same time the turn on field decreases as the

gas pressure decreases. In the vacuum condition, the field enhancement factor is high as expected.

Furthermore, the FN curves show some slight 'knee' with lower background gas pressure. By compare the β value, we found the field enhancement value which we got from the dry air background gas ambiance is a little bit higher than in helium. So we can get the conclusion that before the current got some critical value like saturation current. The atom in the background gas may attract some of the electrons who are supposed to get to the anode. Then the current we collected in this case is lower than the same sample tested in vacuum ambiance.

We also found that the growth time is still the most importance condition which affects the field enhancement factor. From the Table 4.14 we could found when the tube is long enough the field enhancement factor increase more greatly with the decrease background gas pressure than the shorter tubes.

Table 4.14 Field emission and enhancement of samples with 5 min sputtering times 20 min and 120 min growth times in various dry air pressures.

Sample name	Slope Coefficient	Field Enhancement factor	turn on field (V/μm)
	k_1	β_1	
5-20 2e-2	-52.07	1252	2.93
5-20 2e-4	-47.02	1387	2.57
5-20 2e-5	-53.56	1217	2.36
5-20 2e-6	-20.5	3180	2.28
5-120 2e-2	-22.55	2891	1.57
5-120 2e-4	-16.9	3858	1.21
5-120 2e-5	-10.99	5933	0.96
5-120 2e-6	-10.21	6386	0.86

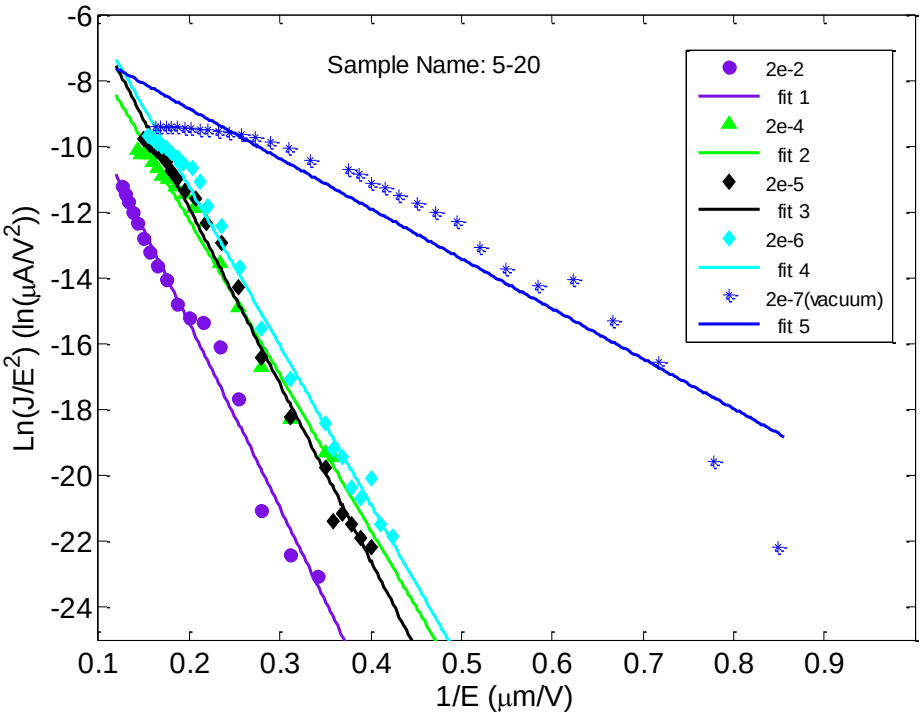

Fig 4.16: FN plots with 5 min sputtering time and 20 min growth time under various dry air field emission test background gas pressures

CHAPTER 5

SUMMARY AND CONCLUSIONS

Randomly oriented carbon nanotubes (CNTs) are fabricated using chemical vapor deposition (CVD) under different sputtering and growth conditions. It is not shown here, but the SEM images show that as growth time increases the length of the (CNTs) increase, and the aspect ratio increases [60]. Field emission characteristics of these samples are recorded in vacuum and higher pressures. The results show that as the growth time increases, lower turn-on fields are achieved. We also observe that as pressure increase, the turn on field increases. Using the field emission data, F-N Curves are plotted and the field enhancement factor β of each sample is determined to be nonlinear. Therefore two distinct classifications of the field enhancement factor are defined; one in low field region and the other in high field region. It is observed that the low field enhancement factor increases as the growth time increases. On the other hand, the samples with 240 min growth time have a lower field enhancement factor than the samples with 120 min growth time. We speculate that because the nanotubes are randomly oriented, if the tube lengths are too long (in the case of 240 min growth time) they may be entangled decreasing the aspect ratio and result in poor field emission.

Samples are also tested in higher pressures. We observed that the field enhancement factor decreases as the background pressure increases. This is an expected result, because the quantum tunneling process for the field emission is

defined only for vacuum pressures. The atoms in the background gas significantly affected the electrons quantity reach the anode which used to collect electrons come from field emission process. The results are preliminary, and full analysis is needed to explain the fundamental processes of non-linear behavior of the field enhancement factor.

Samples of CNTs grown on silicon dioxide and Titanium underlying layer also been tested in high vacuum ambiance (1×10^{-7} Torr). All the samples grown on underlying layer have the same grown time 20 min. I compared all the samples with different catalyst (iron) sputtering time. In generally, the turn on field will decrease and the field enhancement factor will increased with the sputtering time increase. In other word, the longer sputtering time always lead better field emission result for the samples grown on pure silicon and silicon dioxide. While the samples grown on Ti underlying layer exhibit totally opposite trend whose turn on field increased with the sputtering time increased. So we can get the conclusion that there must be an optimized thickness of catalyst for different kinds of substrates.

REFERENCE

[1] J. Oh, K. Lee, T. Lee, C. Yang, and H. Corporation, "Thermal and crystallization behaviors of thin-MWCNT/Polyamide 6 Nanocomposite," *Nature*, vol. 56, no. 354, pp. 13–14, 1991.

[2] R. Seelaboyina, S. Boddepalli, K. Noh, M. Jeon, and W. Choi, "Enhanced field emission from aligned multistage carbon nanotube emitter arrays.," *Nanotechnology*, vol. 19, no. 6, p. 065605, Feb. 2008.

[3] J. Zhang, G. Yang, Y. Cheng, B. Gao, Q. Qiu, Y. Z. Lee, J. P. Lu, and O. Zhou, "Stationary scanning x-ray source based on carbon nanotube field emitters," *Applied Physics Letters*, vol. 86, no. 18, p. 184104, 2005.

[4] G. Chen, D. H. Shin, S. Kim, S. Roth, and C. J. Lee, "Improved field emission stability of thin multiwalled carbon nanotube emitters.," *Nanotechnology*, vol. 21, no. 1, p. 015704, Jan. 2010.

[5] M. Endo, T. Hayashi, and Y.-A. Kim, "Large-scale production of carbon nanotubes and their applications," *Pure and Applied Chemistry*, vol. 78, no. 9, pp. 1703–1713, 2006.

[6] T. W. Ebbesen, H. Hiura, J. Fujita, Y. Ochiai, S. Matsui, and K. Tanigaki, "Patterns in the bulk growth of carbon nanotubes," *Chemical Physics Letters*, vol. 209, no. 1–2, pp. 83–90, Jun. 1993.

[7] H. Dai, "Carbon nanotubes: synthesis, integration, and properties.," *Accounts of chemical research*, vol. 35, no. 12, pp. 1035–44, Dec. 2002.

[8] W. B. Choi, D. S. Chung, J. H. Kang, H. Y. Kim, Y. W. Jin, I. T. Han, Y. H. Lee, J. E. Jung, N. S. Lee, G. S. Park, and J. M. Kim, "Fully sealed, high-brightness carbon-nanotube field-emission display," *Applied Physics Letters*, vol. 75, no. 20, p. 3129, 1999.

[9] Z. Liu, G. Yang, Y. Z. Lee, D. Bordelon, J. Lu, and O. Zhou, "Carbon nanotube based microfocus field emission x-ray source for microcomputed tomography," *Applied Physics Letters*, vol. 89, no. 10, p. 103111, 2006.

[10] W. I. Milne, K. B. K. Teo, E. Minoux, O. Groening, L. Gangloff, L. Hudanski, J.-P. Schnell, D. Dieumegard, F. Peauger, I. Y. Y. Bu, M. S. Bell, P. Legagneux, G. Hasko, and G. a. J. Amaratunga, "Aligned carbon nanotubes/fibers for applications in vacuum microwave amplifiers," *Journal of Vacuum Science & Technology B: Microelectronics and Nanometer Structures*, vol. 24, no. 1, p. 345, 2006.

[11] H. Zhao, "Design and Construction of Carbon NanoTubes (CNTs) Triggered Pseudospark Switch," 2012.

[12] A. Teng, "Physical Properties of Carbon Nanotubes Physical Properties of Carbon Nanotubes," 2010.

[13] R. C. Batra and a. Sears, "Continuum models of multi-walled carbon nanotubes," *International Journal of Solids and Structures*, vol. 44, no. 22–23, pp. 7577–7596, Nov. 2007.

[14] C. Shen, A. H. Brozena, and Y. Wang, "Double-walled carbon nanotubes: challenges and opportunities.," *Nanoscale*, vol. 3, no. 2, pp. 503–18, Feb. 2011.

[15] M. J.O'Connell, *Carbon Nanotubes: Properties and Applications*. CRC Press, 2006.

[16] Carsten Winter, "Time-resolved electron spectroscopy in Graphene with High Harmonic radiation." .

[17] M. S. Dresselhaus, G. Dresselhaus, J. C. Charlier, and E. Hernández, "Electronic, thermal and mechanical properties of carbon nanotubes.," *Philosophical transactions. Series A, Mathematical, physical, and engineering sciences*, vol. 362, no. 1823, pp. 2065–98, Oct. 2004.

[18] M. Terrones, "SCIENCE AND T ECHNOLOGY OF THE T WENTY -F IRST C ENTURY : Synthesis, Properties, and Applications of Carbon Nanotubes," *Annual Review of Materials Research*, vol. 33, no. 1, pp. 419–501, Aug. 2003.

[19] P. Avouris, "Carbon Nanotube Electronics and Optoelectronics," no. 3, pp. 403–410, 2004.

[20] Qing Zhang, *Carbon Nanotubes and Their Applications*. Pan Stanford Publishing Pte. Ltd., 2012.

[21] T.W.Ebbesen, *Carbon Nanotubes: preparation and properties*. CRC Press, 1997.

[22] and H. H. P. M Ajayan, T. W. Ebbesen, T. Ichihashi, , S. Iijima., K. Tanigaki, "Opening carbon nanotubes with oxygen and implications for filling," *Nature*, vol. 362, no. 8, 1993.

[23] T. W. E. and K. T. Hidefumi Hiura, "Opening and purification of carbon nanotubes in high yields," *Adv.Mater*, vol. 7, no. 3, pp. 275–276, 1995.

[24] R. Bokka, “Carbon nanotube Cold Cathodes for Applications under Vacuum to Partial Pressure in Helium and Dryair,” Auburn, 2011.

[25] R. S. Ruoff, D. Qian, and W. K. Liu, “Mechanical properties of carbon nanotubes: theoretical predictions and experimental measurements,” *Comptes Rendus Physique*, vol. 4, no. 9, pp. 993–1008, Nov. 2003.

[26] P. R. Bandaru, “Electrical Properties and Applications of Carbon Nanotube Structures,” *Journal of Nanoscience and Nanotechnology*, vol. 7, no. 4, pp. 1239–1267, Apr. 2007.

[27] C.-N. Tsai, “Selective and Non-selective Synthesis of Carbon Nanotubes (CNTs) by Chemical Vapor Deposition (CVD) Characterization: Catalysts and Underlayers E ects on Field Emission Properties,” 2012.

[28] M. A. J. V. M.Daenen, R.D.de Fouw, B.Hamers, P.G.A. Janssen, K.Schouteden, “The Wondrous World of Carbon Nanotubes,” 2003.

[29] R. T. K. B. and P. S. Harris, “No Title,” *Chemistry and Physics of Carbon*, vol. 14, p. 83, 1978.

[30] R. T. K. Baker, P. S. Harris, R. B. Thomas, and R. J. Waite, “Formation of filamentous carbon from iron, cobalt and chromium catalyzed decomposition of acetylene,” *Journal of Catalysis*, vol. 30, no. 1, pp. 86–95, 1973.

[31] C. Bower, O. Zhou, W. Zhu, D. J. Werder, and S. Jin, “Nucleation and growth of carbon nanotubes by microwave plasma chemical vapor deposition,” *Applied Physics Letters*, vol. 77, no. 17, p. 2767, 2000.

[32] a. Gohier, C. P. Ewels, T. M. Minea, and M. a. Djouadi, “Carbon nanotube growth mechanism switches from tip- to base-growth with decreasing catalyst particle size,” *Carbon*, vol. 46, no. 10, pp. 1331–1338, Aug. 2008.

[33] J. Zhang, G. Yang, Y. Z. Lee, S. Chang, J. P. Lu, and O. Zhou, “Multiplexing radiography using a carbon nanotube based x-ray source,” *Applied Physics Letters*, vol. 89, no. 6, p. 064106, 2006.

[34] C. Li, Y. Zhang, M. Mann, D. Hasko, W. Lei, B. Wang, D. Chu, D. Pribat, G. a. J. Amaratunga, and W. I. Milne, “High emission current density, vertically aligned carbon nanotube mesh, field emitter array,” *Applied Physics Letters*, vol. 97, no. 11, p. 113107, 2010.

[35] W. B. Choi, D. S. Chung, J. H. Kang, H. Y. Kim, Y. W. Jin, I. T. Han, Y. H. Lee, J. E. Jung, N. S. Lee, G. S. Park, and J. M. Kim, “Fully sealed, high-brightness carbon-nanotube field-emission display,” *Applied Physics Letters*, vol. 75, no. 20, p. 3129, 1999.

[36] E. L. Murphy and R. H. Good, “Thermionic Emission, Field Emission, and the Transition Region,” vol. 102, no. 1955, 1956.

[37] B. Padya, D. Kalita, P. K. Jain, G. Padmanabham, M. Ravi, and K. S. Bhat, "Self-organized growth of bamboo-like carbon nanotube arrays for field emission properties," *Applied Nanoscience*, vol. 2, no. 3, pp. 253–259, Apr. 2012.

[38] R. G. Forbes, "Refining the application of Fowler Nordheim theory," vol. 79, no. February, pp. 11–23, 1999.

[39] R. H. Fowler and L. Nordheim, "Electron Emission in Intense Electric Fields," *Proceedings of the Royal Society A: Mathematical, Physical and Engineering Sciences*, vol. 119, no. 781, pp. 173–181, May 1928.

[40] R. G. Forbes, "Physics of generalized Fowler-Nordheim-type equations," *Journal of Vacuum Science & Technology B: Microelectronics and Nanometer Structures*, vol. 26, no. 2, p. 788, 2008.

[41] P. Y. Chen, T. C. Cheng, J. H. Tsai, and Y. L. Shao, "Space charge effects in field emission nanodevices.," *Nanotechnology*, vol. 20, no. 40, p. 405202, Oct. 2009.

[42] X. Lu, Q. Yang, C. Xiao, and a Hirose, "Nonlinear Fowler–Nordheim plots of the field electron emission from graphitic nanocones: influence of non-uniform field enhancement factors," *Journal of Physics D: Applied Physics*, vol. 39, no. 15, pp. 3375–3379, Aug. 2006.

[43] Y. Feng and J. P. Verboncoeur, "Transition from Fowler-Nordheim field emission to space charge limited current density," vol. 073105, no. 2006, 2012.

[44] Y. W. Zhu, H. Z. Zhang, X. C. Sun, S. Q. Feng, J. Xu, Q. Zhao, B. Xiang, R. M. Wang, and D. P. Yu, "Efficient field emission from ZnO nanoneedle arrays," *Applied Physics Letters*, vol. 83, no. 1, p. 144, 2003.

[45] S. Li, "Cold Cathode Materials for Pseudospark Switches," 2010.

[46] L. Nilsson, "Field emission from carbon nanotubes : the first five years," vol. 45, 2001.

[47] and D. U. W.de Heer, A. Charelain, "A carbon nanotube field-emission electron source," *Science*, vol. 207, no. 1179, 1995.

[48] J. L. Silan, D. L. Niemann, B. P. Ribaya, M. Rahman, M. Meyyappan, and C. V. Nguyen, "Carbon nanotube pillar arrays for achieving high emission current densities," *Applied Physics Letters*, vol. 95, no. 13, p. 133111, 2009.

[49] S. Fujii, S. Honda, H. Machida, H. Kawai, K. Ishida, M. Katayama, H. Furuta, T. Hirao, and K. Oura, "Efficient field emission from an individual aligned carbon nanotube bundle enhanced by edge effect," *Applied Physics Letters*, vol. 90, no. 15, p. 153108, 2007.

[50] J. L. Killian, N. B. Zuckerman, D. L. Niemann, B. P. Ribaya, M. Rahman, R. Espinosa, M. Meyyappan, and C. V. Nguyen, "Field emission properties of carbon nanotube pillar arrays," *Journal of Applied Physics*, vol. 103, no. 6, p. 064312, 2008.

[51] J. Bonard, T. Stora, J. Salvetat, F. Maier, T. Stöckli, and C. Duschl, "Purification and size-selection of carbon nanotubes," vol. 9, no. 10, pp. 1–5, 1997.

[52] J.-M. Bonard, J.-P. Salvetat, T. Stöckli, W. a. de Heer, L. Forró, and A. Châtelain, "Field emission from single-wall carbon nanotube films," *Applied Physics Letters*, vol. 73, no. 7, p. 918, 1998.

[53] L. Chen, Z. Ji, Y. Mi, H. Ni, and H. Zhao, "Nonlinear characteristics of the Fowler–Nordheim plots of carbon nanotube field emission," *Physica Scripta*, vol. 82, no. 3, p. 035602, Sep. 2010.

[54] L. F. Chen, H. Song, L. Z. Cao, H. Jiang, D. B. Li, W. G. Guo, X. Liu, H. F. Zhao, and Z. M. Li, "Effect of interface barrier between carbon nanotube film and substrate on field emission," *Journal of Applied Physics*, vol. 106, no. 3, p. 033703, 2009.

[55] X. L. Jihua Zhang, Chuanren Yang, Wenwei Yang Tao Feng, Xi Wang, "Appearance of a knee on the Fowler-Nordheim plot of carbon nanotubes on a substrate," *Solid State Communications*, vol. 138, pp. 13–16, 2006.

[56] S. J. Tans, A. R. M. Verschueren, and C. Dekker, "Room-temperature transistor based on a single carbon nanotube," *Nature*, vol. 672, no. 1989, pp. 669–672, 1998.

[57] J. Bonard, J. Salvetat, T. Stöckli, and L. Forr, "Field emission from carbon nanotubes : perspectives for applications," vol. 254, pp. 245–254, 1999.

[58] T. Guo, P. Nikolaev, A. G. Rinzler, D. Tombnek, D. T. Colbert, and R. E. Smalley, "Self-Assembly of Tubular Fullerenes," pp. 10694–10697, 1995.

[59] "unraveling nanotube field emission from an atomic wire.pdf," *Science*, vol. 269, no. 5230, pp. 1550–1553, 1995.

[60] "carbon nanotube cold cathodes for applications under vacuum to partial pressure in Helium and Dryair," 2011.

[61] L. T. Williams, V. S. Kumsomboone, W. J. Ready, S. Member, and M. L. R. Walker, "Lifetime and Failure Mechanisms of an Arrayed Carbon Nanotube Field Emission Cathode," vol. 57, no. 11, pp. 3163–3168, 2010.

[62] R. Gomer, *Field Emission and Field Ionization*. 1961.

APPENDICES

LIST OF ALL THE FIELD EMISSION TEST SAMPLES

Name of Samples	Underlying Layer	catalyst	Growth time (mins)	Sputtering time (mins)	Test pressure (Torr)	Back ground gas	Name of Table
5-10	N/A	Iron	10	5	2.0E-07	N/A	Table 4.1
5-20	N/A	Iron	20	5	2.0E-07	N/A	Table 4.1
5-40	N/A	Iron	40	5	2.0E-07	N/A	Table 4.1
5-80	N/A	Iron	80	5	2.0E-07	N/A	Table 4.1
5-120	N/A	Iron	120	5	2.0E-07	N/A	Table 4.1
5-240	N/A	Iron	240	5	2.0E-07	N/A	Table 4.1
10-10	N/A	Iron	10	10	2.0E-07	N/A	Table 4.2
10-20	N/A	Iron	20	10	2.0E-07	N/A	Table 4.2
10-40	N/A	Iron	40	10	2.0E-07	N/A	Table 4.2
10-80	N/A	Iron	80	10	2.0E-07	N/A	Table 4.2
10-120	N/A	Iron	120	10	2.0E-07	N/A	Table 4.2
10-240	N/A	Iron	240	10	2.0E-07	N/A	Table 4.2
Fe5SiO2	Oxide(0.6µm)	Iron(<7nm)	20	5	2.0E-07	N/A	Table 4.4
Fe10SiO2	Oxide(0.6µm)	Iron(≈10nm)	20	10	2.0E-07	N/A	Table 4.4
Fe5Ti	Titanium(0.6µm)	Iron(<7nm)	20	5	2.0E-07	N/A	Table 4.5
Fe10Ti	Titanium(0.6µm)	Iron(<7nm)	20	10	2.0E-07	N/A	Table 4.5

List of all the field emission test samples (Continue)

Name of Samples	Underlying Layer	catalyst	Growth time (mins)	Sputtering time (mins)	Test pressure (Torr)	Back ground gas	Name of Table
He 5-10	N/A	Iron	10	5	2.0E-02	Helium	Table 4.6
He 5-20	N/A	Iron	20	5	2.0E-02	Helium	Table 4.6
He 5-40	N/A	Iron	40	5	2.0E-02	Helium	Table 4.6
He 5-80	N/A	Iron	80	5	2.0E-02	Helium	Table 4.6
He 5-120	N/A	Iron	120	5	2.0E-02	Helium	Table 4.6
He 5-240	N/A	Iron	240	5	2.0E-02	Helium	Table 4.6
He 10-20	N/A	Iron	20	10	2.0E-02	Helium	Table 4.7
He 10-80	N/A	Iron	80	10	2.0E-02	Helium	Table 4.7
He 5-20 2e-2	N/A	Iron	20	5	2.0E-02	Helium	Table 4.8
He 5-20 2e-4	N/A	Iron	20	5	2.0E-04	Helium	Table 4.8
He 5-20 2e-5	N/A	Iron	20	5	2.0E-05	Helium	Table 4.8
He 5-20 2e-6	N/A	Iron	20	5	2.0E-06	Helium	Table 4.8
vacuum 5-20	N/A	Iron	20	5	2.0E-07	N/A	Table 4.8
He 10-20 2e-2	N/A	Iron	20	10	2.0E-02	Helium	Table 4.9
He 10-20 2e-4	N/A	Iron	20	10	2.0E-04	Helium	Table 4.9
He 10-20 2e-5	N/A	Iron	20	10	2.0E-05	Helium	Table 4.9
He 10-20 2e-6	N/A	Iron	20	10	2.0E-06	Helium	Table 4.9
vacuum 10-20	N/A	Iron	20	10	2.0E-07	N/A	Table 4.9
He 5-80 2e-2	N/A	Iron	80	5	2.0E-02	Helium	Table 4.10
He 5-80 2e-4	N/A	Iron	80	5	2.0E-04	Helium	Table 4.10
He 5-80 2e-5	N/A	Iron	80	5	2.0E-05	Helium	Table 4.10
He 5-80 2e-6	N/A	Iron	80	5	2.0E-06	Helium	Table 4.10
vacuum 5-80	N/A	Iron	80	5	2.0E-07	N/A	Table 4.10

List of all the field emission test samples (Continue)

Name of Samples	Underlying Layer	catalyst	Growth time (mins)	Sputtering time (mins)	Test pressure (Torr)	Back ground gas	Name of Table
He 10-80 2e-2	N/A	Iron	80	10	2.0E-02	Helium	Table 4.11
He 10-80 2e-4	N/A	Iron	80	10	2.0E-04	Helium	Table 4.11
He 10-80 2e-5	N/A	Iron	80	10	2.0E-05	Helium	Table 4.11
He 10-80 2e-6	N/A	Iron	80	10	2.0E-06	Helium	Table 4.11
vacuum 10-80	N/A	Iron	80	10	2.0E-07	N/A	Table 4.11
5-10	N/A	Iron	10	5	2.0E-02	Dry Air	Table 4.12
5-20	N/A	Iron	20	5	2.0E-02	Dry Air	Table 4.12
5-40	N/A	Iron	40	5	2.0E-02	Dry Air	Table 4.12
5-80	N/A	Iron	80	5	2.0E-02	Dry Air	Table 4.12
5-120	N/A	Iron	120	5	2.0E-02	Dry Air	Table 4.12
5-240	N/A	Iron	240	5	2.0E-02	Dry Air	Table 4.12
5-20 2e-2	N/A	Iron	20	5	2.0E-02	Dry Air	Table 4.14
5-20 2e-4	N/A	Iron	20	5	2.0E-04	Dry Air	Table 4.14
5-20 2e-5	N/A	Iron	20	5	2.0E-05	Dry Air	Table 4.14
5-20 2e-6	N/A	Iron	20	5	2.0E-06	Dry Air	Table 4.14
5-120 2e-2	N/A	Iron	120	5	2.0E-02	Dry Air	Table 4.14
5-120 2e-4	N/A	Iron	120	5	2.0E-04	Dry Air	Table 4.14
5-120 2e-5	N/A	Iron	120	5	2.0E-05	Dry Air	Table 4.14
5-120 2e-6	N/A	Iron	120	5	2.0E-06	Dry Air	Table 4.14